Orbital and spin phase-resolved spectroscopy of the intermediate polar EX Hya using *XMM–Newton* data

Y. Pekön[★] and Ş. Balman[★]

Department of Physics, Middle East Technical University, İnönü Bulvarı, Ankara 06531, Turkey

ABSTRACT

We present the orbital phase-resolved spectra of an intermediate polar, EX Hya, together with the spin phase-resolved spectra during two different epochs using the *X-ray Multi-Mirror Mission* (*XMM–Newton*), European Photon Imaging Camera (pn instrument). We find that the source at the two epochs has the same X-ray luminosity of $\sim 6.5 \times 10^{31}$ erg s^{-1}. We detect spectral variations between the 2000 and 2003 observations of the source. We fitted the spectrum using a neutral hydrogen absorption model with or without covering fraction together with Gaussians for emission lines, two collisional equilibrium plasma emission models (MEKAL) and a cooling-flow plasma emission model (VMCFLOW). We find that two of the three emission components ($kT = 0.6$–0.8 and 1.3–1.7 keV) fitted by the MEKAL models are almost constant over the spin and orbital phases and also over the two different epochs with the normalization varying directly proportional to the flux when the data are folded according to the orbital and spin phase indicating that the slight variation may be due to occultation. The emission modelled by the VMCFLOW changes over the spin and orbital phases and the 2000 and 2003 observations reveal two different ranges of temperatures (3–33 and 8–61 keV, respectively) that model the shock zone in the accretion column(s). The ratios of the spin maximum to minimum and the orbital maximum to minimum spectra along with the increase in the plasma temperatures indicate that the spectrum gets harder in the minimum phases of both orbital and spin periods. In the 2003 observation, a 6.4 keV fluorescent Fe emission line is present at the orbital minima in a range of phases from 0.9 to 1.3 and it is absent otherwise. This indicates that there is reflection from the disc most likely from a large bulge at the accretion impact zone.

Key words: binaries: close – stars: individual: EX Hya – stars: rotation – white dwarfs – X-rays: stars.

1 INTRODUCTION

Cataclysmic variables (CVs) are compact binaries hosting a white dwarf (WD) primary star accreting material from the hydrogen-rich companion. The accretion occurs through an accretion disc in cases where the magnetic field of the WD is weak ($B < 0.01$ MG) and such systems are referred to as non-magnetic CVs. The magnetic CVs (mCVs) constitute about 25 per cent of the entire population of CVs. There are two subclasses depending on magnetic field strength. Polars (AM Her type systems) have $B > 10$ MG where this strong field causes the accretion flow to directly channel on to the magnetic pole of the WD inhibiting the creation of an accretion disc (see Cropper 1990; Warner 2003). Polars show strong

circular and linear polarization modulated at P_{orb} and the WD rotation P_{spin} is synchronized with the binary orbit. Only about 1 per cent of the polars are found to show asynchronicity. The second class of mCVs are intermediate polars (IPs; DQ Her type systems) that have a weaker field strength compared with polars of about 1–10 MG. In this case, the accretion takes place via a truncated disc to the magnetic poles through accretion curtains. Near the surface of the WD, the accreting material forms a strong shock where the post shock region heats up to 10–20 keV and then cools via thermal bremsstrahlung (Paterson 1994; Hellier 1996; de Martino et al. 2008; Brunschweiger et al. 2009). IPs are asynchronous systems where the orbital period of the system P_{orb} is larger than the spin period of the WD P_{spin}. The majority of the IPs have $P_{spin}/P_{orb} < 0.1$, theoretically they are predicted to lie in the 0.01–0.6 range (Norton, Wynn & Somerscales 2004; Norton et al. 2008; Scaringi et al. 2010). IPs are well characterized by high complex absorption in their X-ray spectra which extends, where the spectra are available in some

★E-mail: yakup@astroa.physics.metu.edu.tr (YP); solen@astroa.physics.metu.edu.tr (ŞB)

cases, out to 100 keV. They show modulation of the X-ray and/or optical light curves at P_{spin} and the appearance of the beat period (where $1/P_{beat} = 1/P_{spin} - 1/P_{orb}$) or its sidebands. Many mCVs are detected by *INTEGRAL*/Imager on Board the *INTEGRAL* Satellite (IBIS; Barlow et al. 2006; Landi et al. 2009) and *Swift*/Burst Alert Telescope (BAT; Brunschweiger et al. 2009) in the 20–100 keV ranges and most of them are found to be IPs. This is thought to be because the hardest X-ray emission comes from the cooling post-shock region of IPs rather than polars, since the strong magnetic field of polars causes the cyclotron cooling to dominate the cooling post-shock region suppressing the bremsstrahlung emission.

EX Hya was discovered by Kraft (1962) with an orbital period of 98 min. Later, the 67-min rotation period of the WD was identified (Vogt, Krzeminski & Sterken 1980), classifying the source as an IP. The WD mass is estimated to be in the range of 0.5–0.8 M$_\odot$ as measured using optical (Hellier et al. 1987; Beuermann et al. 2003) and X-ray (Fujimoto & Ishida 1997) observations. The elemental abundances are in accordance with solar abundances except for iron which is less than solar (0.6 ± 0.2) (Fujimoto & Ishida 1997). Using optical observations, the system has been found to be at a distance of 64.5 ± 1.2 pc, with a quiescent accretion luminosity of $(2.6 \pm 0.6) \times 10^{32}$ erg s^{-1}, a quiescent accretion rate of $(6.2 \pm 1.5) \times 10^{-11}$ M$_\odot$ yr^{-1} and an inclination of $76\overset{\circ}{.}0$–$77\overset{\circ}{.}6$ (Beuermann et al. 2003).

EX Hya shows a partial eclipse in its light curves over the orbital period. The eclipse was explained by two scenarios: either occultation of one of the poles for two-pole accretion or partial occultation of the accretion column by the secondary for one-pole accretion (Rosen, Mason & Cordova 1988). The source is suggested to have an extended bulge on the outer accretion disc and extended/overflowing material originating from the hotspot (Belle et al. 2005). The source is observed both in outburst and quiescence. During the outburst stage, the Doppler tomograms and radial velocities indicate that the source shows disc overflow and dips in the optical light curve (Mhlahlo et al. 2007b); the disc overflow is also present in the quiescent state (Mhlahlo et al. 2007a) consistent with the above scenario. The evidence of a bulge on the accretion disc is also present in the X-ray observations. The X-ray binary light curves in the 1–20 Å range show an extended broad absorption associated with the disc which increases as the wavelength increases (Hoogerwerf, Brickhouse & Mauche 2005).

The X-ray spectrum of the post-shock emission of EX Hya has been previously modelled with multitemperature plasma emission models. One example uses four optically thin plasma emission models at four different temperatures (Allan, Hellier & Beardmore 1998). Another approach uses a cooling-flow model (MKCFLOW) assuming a multitemperature thermal plasma emission with a relatively flat emission measure distribution indicating cooling gas from a steady-state condition (Mukai et al. 2003).

The spin modulation of the X-ray light curve of the source can be explained either by the absorption difference over the spin phase because of the accretion curtain, or occultation of the accretion curtain by the WD. The occultation scenario is more favoured because the system has tall accretion columns (~ 1 R_{WD}; Allan et al. 1998). The source also shows spectral variability as a function of orbital phase due to absorption (Cropper et al. 2002), but the modulations and spectral models have not been thoroughly investigated until this work.

In this work, the X-ray spectral properties of EX Hya are thoroughly investigated. In Section 2, the X-ray observations and data preparation are introduced. In Section 3, the total spectrum for the 2000 and 2003 data are investigated. A composite-model fit for both

observations is performed and the variation of the spectral parameters between the two observations is discussed. In Section 4, the characteristics of the source spectra in both 2000 and 2003 observations are studied over the orbital phase. The trends in the derived spectral parameters as a function of the orbital phase as well as the differences between the 2000 and 2003 data are compared. In Section 5, a similar analysis is made, this time as a function of the spin phase of EX Hya. In Section 6, the results are discussed and finally in Section 7, the summary and conclusion of our work is presented.

2 OBSERVATION AND DATA

Two different archival observations of EX Hya obtained with the *XMM–Newton* Observatory were used in this study. The first one was conducted on 2000 July 1 (OBS ID: 00111020101) with 30 ks exposure time and the second one on 2003 January 11 (OBS ID: 0057740301) with 57 ks exposure time. The *XMM–Newton* Observatory (Jansen et al. 2001) has a pn CCD detector (Strüder et al. 2001) and two MOS CCD detectors (Turner et al. 2001) sensitive in the 0.2–15 keV energy range at the focus of three European Photon Imaging Cameras (EPIC) with a field of view of about half a degree for each. It also has Reflecting Grating Spectrometers (RGS; den Herder et al. 2001), a high-resolution spectrometer working together with the EPIC detectors sensitive in the 0.35–2.5 keV energy range as well as a 30 cm optical monitor (OM) instrument with an optical/ultraviolet (UV) telescope (Mason et al. 2001).

We first checked the pile up in the observations using EPATPLOT[1] tool in SAS. The EPIC MOS data were piled up in the 2000 observation, hence only EPIC pn data were used for both observations in this analysis. The 2000 observation was a pointed observation of the source in the small window mode for the EPIC pn with a net count rate of 40.1 ± 0.04 count s^{-1} in the 0.2–10 keV energy interval. In the 2003 observation the EPIC pn was used in the extended full frame mode and the source is off axis by 14 arcmin, the net source count rate is 9.7 ± 0.01 count s^{-1} in the 0.2–10 keV energy range. The significantly lower count rate in the 2003 observation is due to vignetting, caused by the source being off-axis. We utilized the CALVIEW tool in SAS and determined the percentage of loss in the count rate as 65 per cent which yields a count rate of about 13–14 count s^{-1} based on 40.1 count s^{-1} from 2000. This is in accordance with our count rate derived from the 2003 data. However, we note a difference of about 30–40 per cent between the rate calculated from the data and our inspection from CALVIEW using the rate of the 2000 data. This may be a result of extra vignetting (corrected in the analysis) or about 30–40 per cent change in the source count rate, which is not conclusive at this stage.

For both observations, the standard pipeline processed data were used to perform the spectral and temporal analysis using the *XMM–Newton* Science Analysis Software (SAS), version 8.0.0. The source light curve and spectrum extraction are done using the XMMSELECT tool within SAS. In the 2000 observation, a circular photon extraction region was centred on the source with a radius 38.8 arcsec, and a same size region was used for the background extraction centred elsewhere on the image. For the 2003 data, since the source was off-axis, an elliptical region with a semimajor axis of 60 arcsec and a semiminor axis of 23.3 arcsec, orientated at an angle of 320° was used in order to extract the source and background events. Data

---

[1] See http://xmm.esac.esa.int/sas/current/documentation/threads/epatplot.shtml

with single- and double-pixel events, i.e. patterns 0–4 with Flag = 0 options were used. In order to perform spectroscopy, we used the PHASECALC tool in SAS, and created phase columns in the event files using the spin and orbital periods; and spectra were extracted from the event files for a phase interval of 0.1 with iterative calls to the ESPECGET tool in SAS yielding phase-resolved spectra. XSPEC 12.2.1 (Arnaud 1996) was used for further analysis.

3 TOTAL SPECTRUM OF THE SOURCE

Prior to the fitting procedure, spectra were calculated using the extraction criteria described in Section 2 in the energy range of 0.2–10.0 keV. The resulting spectra were grouped so that the minimum counts for each energy bin were 300 for the year 2000 observation and 200 for the year 2003 observation using XSPEC. The fits were conducted in the 0.2–10.0 keV energy band.

The first attempts at fitting the total spectra using XSPEC were done by using a plasma emission model that is in collisional equilibrium (MEKAL model in XSPEC) and creating a composite model of several MEKAL models to fit the spectra at several different temperatures as suggested by Allan et al. (1998). Although we included up to four different MEKAL model components, the trials yielded fits with reduced χ^2 more than 2. Then a different approach was taken by using a cooing-flow model (the VMCFLOW model in XSPEC) suggested by Mukai et al. (2003) which again failed to yield good fits. Finally, we combined the two methods, using a cooling-flow model (VMCFLOW) together with two different temperature MEKAL models at around 0.64 and 1.6 keV. An absorber model for the interstellar extinction and a partially covering absorber model (TBABS and PCFABS models in XSPEC) was assumed to account for the intervening absorption for both of the observations.

The fits with the multicomponent model yielded fluctuating residuals around particularly the iron line complex at about 6.7 keV. We believe this problem arises from CTI effects around particularly strong lines in the EPIC pn spectrum. Thus, we decided to model the lines separately and decreased the Fe abundance in the VMCFLOW model to 0.2 times the solar abundance and added Gaussian emission lines to the model at 6.7 and 6.9 keV to account for the Feα emission line complex. This procedure enabled us to individually model the Fe emission lines. We investigated any effects of the reduction of the Fe abundance in modelling the spectra and we detected no other effects. This is expected since the VMCFLOW models only the harder part of the spectra. Other Gaussian emission lines were included in the fitted composite model at 7.8, 0.58 and 0.78 keV for the 2000 data and 7.8, 6.4 and 0.58 keV for the 2003 data in order to reduce the high sigma deviations in the residuals. The 7.8, 0.58 and 0.78 keV lines correspond to Fexxv Kβ, O vii and O viii transitions, respectively, according to the CHIANTI atomic data base. Modelling these lines by increasing the related element abundances is not possible, hence Gaussian profiles are used instead. The fitted spectra are presented in Fig. 1 and the spectral parameters are displayed in Table 1.

We calculate unabsorbed fluxes with similar values of 1.43×10^{-10} and 1.24×10^{-10} erg cm^{-2} s^{-1} for 2000 and 2003 observations, respectively. These flux values yield luminosities of 6.7×10^{31} and 5.8×10^{31} erg s^{-1} assuming a 64.5 pc source distance. Using the relation $L = G\dot{M}M/2R$ and taking the mass of the WD as $0.5\,M_\odot$ and radius as $0.95\,R_\odot$ (Beuermann et al. 2003), we find mass accretion rates of 5.75×10^{-11} and $5.0 \times 10^{-11}\,M_\odot$ yr^{-1} for 2000 and 2003 data, respectively.

Both spectra show an unusual feature; an emission line at around 7.8 keV. To investigate this feature more closely, the spectra of the

2000 and 2003 data were fitted over a range of 5–10 keV with a power-law model for the continuum and three Gaussians to model the emission lines at around 6.7, 6.9 and 7.8 keV. The resulting parameters of the continuum and the spectral lines are displayed in Table 2. We find an emission line centred around $7.8^{+0.3}_{-0.3}$ keV with a linewidth $\sigma = 0.06^{+0.06}_{-0.06}$ keV for 2000, and centred around $7.9^{+0.8}_{-0.8}$ with a linewidth $\sigma = 0.5^{+0.3}_{-0.1}$ for 2003 observations. We believe this is the Fe xxv Kβ emission line. The linewidths for the 6.7 keV emission line is similar for both observations. In the 2003 data, the linewidths for 6.9 and 7.8 keV lines are significantly higher.

4 ORBITAL PHASE-RESOLVED SPECTROSCOPY

In this work, a detailed orbital phase-resolved spectroscopy of EX Hya was carried out for the first time. For both observations, 2000 and 2003, phase columns were created using the ephemeris $T_0 = 243\,7699.94179 + 0.068233846(4)E$ given by Hellier & Sproats (1992). Then for each 0.1 phase interval from phase 0 to 1, the spectra were extracted as described in Section 2. The calculated spectra were grouped such that each energy bin contained minimum of 100 counts to improve the statistical quality. The channels below 0.3 and above 10.0 keV were ignored during the fitting procedure to improve the statistical quality of the spectra.

To start with, we calculated the ratio of the maximum to minimum spectrum of the orbital phase-resolved spectra in order to study the effect of absorption/occultation in the system in the two different years. The ratio of the normalized count rate per energy for phases around the orbital maximum (phases between 0.6 and 0.8) to phases around the orbital minimum (phases between 0.9 and 1.1) is plotted against the energy in Fig. 2. Both 2000 and 2003 spectral ratios show clear spectral variation and a power-law decline as the energy increases with ratio values greater than 1 particularly at lower energies. There is a more pronounced steep decline with increasing energy in the year 2003 showing the existence of large-scale absorption difference within the system from orbital maximum to minimum.

As in the case of the fits to the total spectra, models such as single MEKAL (in XSPEC), composite multiple MEKAL or a single VMCFLOW models alone yielded large reduced χ^2 values above 2 during the fitting procedure within XSPEC. Thus, we attempted to fit a combination of a MEKAL model with a VMCFLOW using solar abundances along with a photoelectric absorption model (WABS in XSPEC). However, this approach did not yield good fits either. The Fe emission line complex around 6.7 keV still yielded fluctuating residuals. Thus, we applied the same procedure to reduce the Fe abundance and adding individual Gaussian lines to model the 6.7 and 6.9 keV iron lines when necessary.

In the analysis of the 2000 data, we used a composite model to fit the spectra at different phases comprising of two collisional equilibrium plasma emission models, MEKAL1 and MEKAL2, one cooling-flow plasma emission model, VMCFLOW, a photoelectric absorption model, WABS, and three Gaussians for particular Fe lines. The spectral parameters from the fit results are displayed in Table 3 and selected parameters are plotted against the orbital phase in Fig. 3. The fitted spectra at orbital minimum (phase 0.9) and maximum (phase 0.3) are shown in Fig. 4. For the absorption component, a simple cold absorber was enough to fit the data, hence a partial covering absorber was not used. The column density of neutral hydrogen [absorption parameter (N_H)] shows distinct variation with the orbital phase and indicates an anticorrelation with the orbital flux variations reaching a maximum at the orbital minimum. This clearly
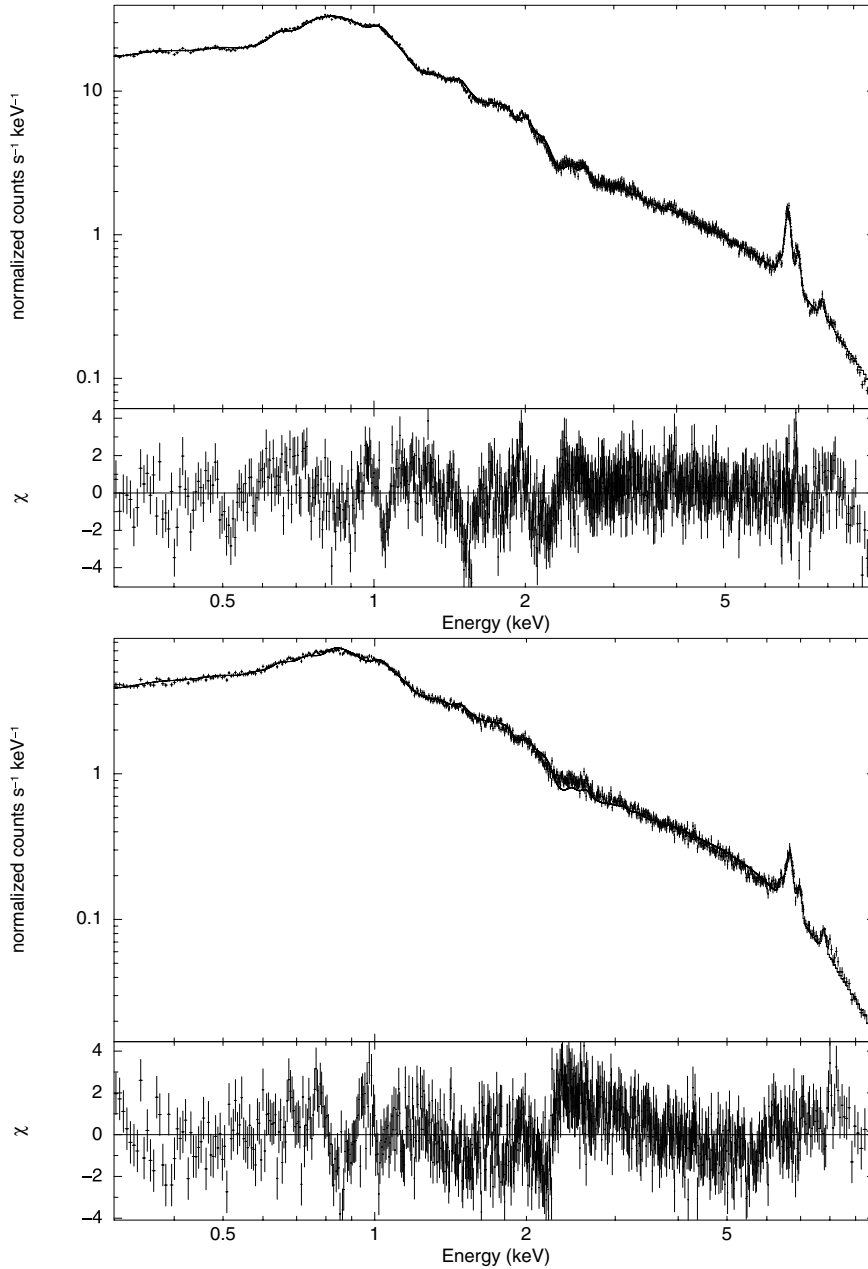
Figure 1. The top panel shows the total EPIC pn spectrum of the year 2000 data (see Table 1 for details). The bottom panel shows the total EPIC pn spectrum of the year 2003 data (see Table 1 for details).

shows that orbital variations at X-ray wavelengths are produced by absorption on the orbital plane. The *LowT* (low temperature) parameter of the VMCFLOW model shows the same anticorrelation with flux and reaches a minimum at orbital maximum, whereas the *HighT* (high temperature) parameter of the same model shows almost a direct correlation with the flux which may imply scattering being at work. The plasma emission components modelled by the MEKAL1 and MEKAL2 models show almost a constant temperature of about 0.6–0.8 and 1.3–1.7 keV and the normalization vary slightly in phase with the orbital motion. The Gaussian line at 6.7 keV does not vary with orbital phase apart from a slight drop between phases 0.6 and 0.7 which indicates that the region where the line is produced is visible at all times during the binary motion.

In the analysis of the 2003 data, we used a composite model comprising two collisional equilibrium plasma emission model, MEKAL1 and MEKAL2, one cooling-flow plasma emission model, VMCFLOW, a photoelectric absorption model, WABS, and three Gaussians for particular Fe lines. The spectral parameters from the fit results are displayed in Table 4 and selected parameters are plotted against the orbital phase in Fig. 5. The fitted spectra at orbital minimum (phase 0) and maximum (phase 0.4) are shown in Fig. 6. The resulting fits have reduced χ^2 well below 2 for all the phase spectra. We find that some parameters show distinct variations with the orbital phase. The N_H parameter for the intrinsic absorption and *LowT* parameter of the VMCFLOW show anticorrelation with the flux, i.e. they yield higher values at orbital minimum phases

Table 1. Spectral parameters of the years 2000 and 2003 observations in the 0.3–10 keV range. Both spectra were fitted with a composite model of two collisional equilibrium plasma emission models at different temperatures (MEKAL), two Gaussians centred at 6.7 and 6.9 keV, a variable cooling-flow plasma emission model (VMCFLOW), a partial covering absorber model (PCFABS) and a simple absorption model (TBABS). For the year 2000 spectrum, three more Gaussians were added at 0.58, 0.78 and 7.8 keV. For the year 2003 spectrum three more Gaussians were added at 6.4, 0.58 and 7.8 keV. $N_{\rm H}$ is the absorbing neutral hydrogen column density, CoverFrac is the covering fraction of the absorber. The given errors correspond to 2σ confidence level for a single parameter. Gaussian line centres were fixed at their best-fitting values and the iron abundance parameter in VMCFLOW was fixed to 0.2 to improve the quality of the fits.

Model	Component	2000 total spectrum	2003 total spectrum
tbabs	$N_{\rm H}$ ($\times 10^{22}$ atoms cm^{-2})	$0.0097^{+0.0007}_{-0.0007}$	$0.0092^{+0.0025}_{-0.0035}$
pcfabs	$N_{\rm H}$ ($\times 10^{22}$ atoms cm^{-2})	$0.86^{+0.17}_{-0.16}$	$0.17^{+0.06}_{-0.04}$
	CoverFrac	$0.22^{+0.01}_{-0.01}$	$0.35^{+0.7}_{-0.5}$
MEKAL1	kT	$0.66^{+0.01}_{-0.01}$	$0.63^{+0.01}_{-0.01}$
	Norm ($\times 10^{-3}$)	$4.8^{+0.2}_{-0.2}$	$2.9^{+0.2}_{-0.1}$
MEKAL2	kT	$1.58^{+0.05}_{-0.05}$	$1.65^{+0.07}_{-0.08}$
	Norm ($\times 10^{-3}$)	$7.8^{+0.7}_{-0.7}$	$4.3^{+0.5}_{-0.5}$
Gaussian1 (6.7 keV)	σ (keV)	$0.070^{+0.006}_{-0.005}$	$0.076^{+0.009}_{-0.010}$
	Norm ($\times 10^{-4}$)	$2.8^{+0.1}_{-0.1}$	$2.6^{+0.2}_{-0.2}$
Gaussian2 (6.9 keV)	σ (keV)	$0.042^{+0.016}_{-0.020}$	$0.064^{+0.035}_{-0.040}$
	Norm ($\times 10^{-5}$)	$6.3^{+0.6}_{-0.6}$	$5.8^{+1.1}_{-1.1}$
Gaussian3 (6.4 keV)	σ (keV)	N/A	$0.11^{+0.04}_{-0.04}$
	Norm ($\times 10^{-5}$)	N/A	$4.5^{+1.1}_{-1.0}$
Gaussian4 (7.8 keV)	σ (keV)	$0.06^{+0.06}_{-0.06}$	$0.51^{+0.29}_{-0.14}$
	Norm ($\times 10^{-5}$)	$2.7^{+1.0}_{-0.7}$	$18.2^{+7.6}_{-4.6}$
Gaussian5 (0.58 keV)	σ (keV)	0 (frozen)	0 (frozen)
	Norm ($\times 10^{-4}$)	$3.9^{+0.6}_{-0.6}$	$5.2^{+0.8}_{-0.8}$
Gaussian6 (0.78 keV)	σ (keV)	0 (frozen)	N/A
	Norm ($\times 10^{-4}$)	$5.0^{+0.6}_{-0.6}$	N/A
VMCFLOW	*LowT*	$3.4^{+0.6}_{-0.6}$	$9.0^{+1.2}_{-1.0}$
	HighT	$29.1^{+3.6}_{-3.4}$	$59.2^{+2.4}_{-2.1}$
	Norm ($\times 10^{-8}$)	$5.9^{+1.0}_{-0.7}$	$2.9^{+0.2}_{-0.1}$
	χ^2_ν	1.70 (956 d.o.f.)	1.66 (903 d.o.f.)

Table 2. Parameters for the common Gaussian emission lines in 2000 and 2003 spectra.

Emission line	Component	2000 spectrum	2003 spectrum
Gaussian1 (6.7 keV)	Peak energy (keV)	6.7 (fixed)	6.7 (fixed)
	σ (keV)	$0.070^{+0.006}_{-0.005}$	$0.076^{+0.009}_{-0.010}$
	Norm ($\times 10^{-4}$)	$2.8^{+0.1}_{-0.1}$	$2.6^{+0.2}_{-0.2}$
Gaussian2 (6.9 keV)	Peak energy (keV)	6.9 (fixed)	6.9 (fixed)
	σ (keV)	$0.042^{+0.016}_{-0.020}$	$0.064^{+0.035}_{-0.040}$
	Norm ($\times 10^{-5}$)	$6.3^{+0.6}_{-0.6}$	$5.8^{+1.1}_{-1.1}$
Gaussian3 (7.8 keV)	Peak energy (keV)	$7.8^{+0.3}_{-0.3}$	$7.9^{+0.8}_{-0.8}$
	σ (keV)	$0.059^{+0.063}_{-0.059}$	$0.51^{+0.29}_{-0.14}$
	Norm ($\times 10^{-5}$)	$2.6^{+1.0}_{-0.7}$	$18.2^{+7.7}_{-4.6}$

(phases between 0.9 and 1.3), and lower values at the maximum phases (phases between 0.4 and 0.8). This indicates that source emission is being absorbed at particular phases (0.9 and 1.3) where there is absorption on the orbital plane and the spectrum gets harder in general (softer X-rays are absorbed). The *HighT* parameter shows no distinct variation over the orbital phase in the 2003 data. This is obvious since harder X-rays will not be affected/absorbed as much by the neutral absorption.

The plasma emission components modelled by the MEKAL model in the 2003 data show almost a constant temperature of about 0.6–0.8 and 1.3–1.7 keV; the normalizations vary slightly in phase with the flux. These components may be affected by only occultation, i.e. the eclipse itself. The width σ and normalization of the 6.7 keV emission line show direct correlation, with low values at orbital minimum and high values at orbital maximum. The 6.7 keV emission line (Fe xxv line) is present at all phases. For the orbital minimum (phases between 0.9 and 1.3), emission lines at 6.9 keV (Fe xxvi line) and at 6.4 keV (fluorescent Fe line) were necessary for successful fits to the data (see Fig. 6). Fig. 7 shows the necessity to include the 6.4 and 6.9 keV emission lines in the 2003 orbital spectra
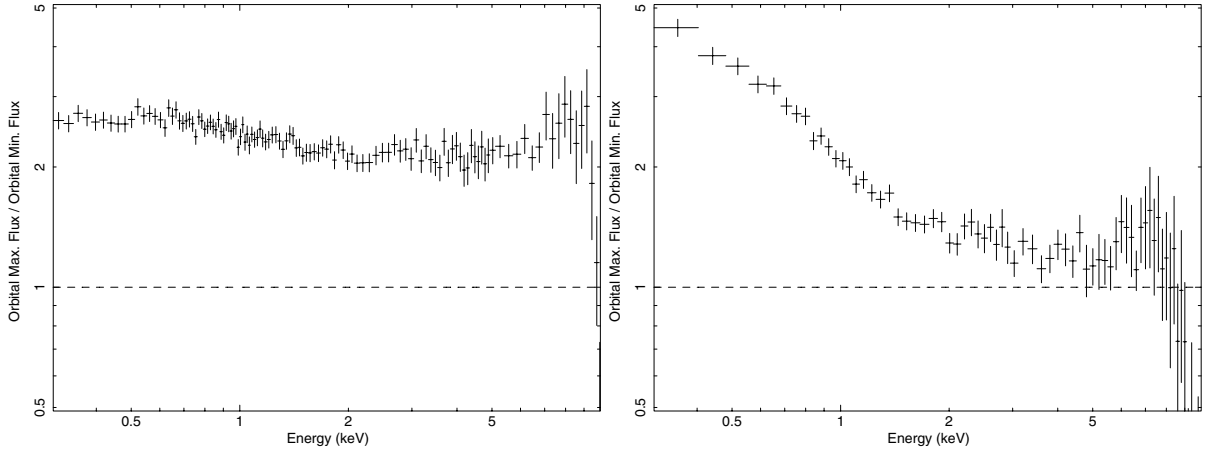
Figure 2. The left-hand panel shows the ratio of the count rate spectrum of the orbital maximum to the spectrum of the orbital minimum in the year 2000 data. The right-hand panel shows the ratio of the count rate spectrum of the orbital maximum to the spectrum of the orbital minimum in the year 2003 data.

Table 3. Spectral parameters derived for the year 2000 observation at each orbital phase of 0.1 in the 0.3–10 keV range. All the spectra were fitted with a composite model of two collisional equilibrium plasma emission models at different temperatures (MEKAL), two Gaussians centred at 6.7 and 6.9 keV, a variable cooling-flow plasma emission model (VMCFLOW) and photoelectric absorption of H I (WABS). The given errors correspond to 2σ confidence level for a single parameter. Gaussian line centres were fixed at their best-fitting values and the iron abundance parameter in VMCFLOW was fixed to 0.2 to improve the quality of the fits.

Model	Component	0.1	0.2	0.3	0.4	0.5
wabs	$N_H(\times 10^{-22})$	$0.035^{+0.002}_{-0.002}$	$0.015^{+0.002}_{-0.002}$	$0.010^{+0.002}_{-0.002}$	$0.013^{+0.002}_{-0.002}$	$0.016^{+0.002}_{-0.003}$
MEKAL1	kT	$0.64^{+0.01}_{-0.01}$	$0.62^{+0.02}_{-0.02}$	$0.63^{+0.01}_{-0.01}$	$0.64^{+0.01}_{-0.01}$	$0.63^{+0.01}_{-0.01}$
	Norm $(\times 10^{-4})$	$3.5^{+0.1}_{-0.1}$	$4.3^{+0.2}_{-0.2}$	$4.7^{+0.2}_{-0.2}$	$4.8^{+0.2}_{-0.2}$	$4.3^{+0.2}_{-0.2}$
MEKAL2	kT	$1.57^{+0.12}_{-0.14}$	$1.37^{+0.06}_{-0.07}$	$1.56^{+0.11}_{-0.13}$	$1.59^{+0.17}_{-0.17}$	$1.60^{+0.13}_{-0.17}$
	Norm $(\times 10^{-4})$	$5.9^{+0.9}_{-0.9}$	$5.6^{+0.2}_{-0.2}$	$7.9^{+1.0}_{-1.1}$	$7.5^{+1.2}_{-1.3}$	$6.4^{+1.2}_{-1.2}$
VMCFLOW	$LowT$	$11.5^{+0.7}_{-0.5}$	$6.1^{+3.0}_{-2.8}$	$6.9^{+0.4}_{-0.4}$	$3.5^{+0.6}_{-0.5}$	$5.1^{+0.9}_{-0.5}$
	$HighT$	$14.7^{+0.8}_{-1.2}$	$18.2^{+9.5}_{-3.1}$	$18.6^{+5.7}_{-3.4}$	$32.8^{+1.0}_{-0.9}$	$29.5^{+1.4}_{-1.2}$
	Norm $(\times 10^{-9})$	$39.4^{+15.7}_{-11.8}$	$12.2^{+5.6}_{-5.6}$	$14.4^{+2.6}_{-3.1}$	$6.1^{+13.7}_{-1.6}$	$6.2^{+1.2}_{-0.7}$
Gaussian1 (6.7 keV)	σ	$0.11^{+0.02}_{-0.02}$	$0.11^{+0.03}_{-0.2}$	$0.11^{+0.04}_{-0.01}$	$0.11^{+0.03}_{-0.02}$	$0.14^{+0.03}_{-0.03}$
	Norm $(\times 10^{-5})$	$2.7^{+0.5}_{-0.3}$	$5.7^{+0.4}_{-0.2}$	$3.2^{+0.5}_{-0.4}$	$3.1^{+0.4}_{-0.4}$	$3.4^{+0.6}_{-0.5}$
Gaussian2 (6.9 keV)	σ	0	0	0	0	0
	Norm $(\times 10^{-6})$	$3.5^{+1.9}_{-2.5}$	$3.6^{+2.0}_{-2.5}$	$3.8^{+2.0}_{-2.5}$	$2.8^{+2.0}_{-2.5}$	$2.6^{+3.0}_{-1.8}$
	χ^2_ν (d.o.f.)	1.35 (510)	1.31 (557)	1.29 (574)	1.29 (585)	1.20 (548)

| Model	Component	0.6	0.7	0.8	0.9	1.0
wabs	$N_H(\times 10^{-22})$	$0.010^{+0.002}_{-0.002}$	$0.016^{+0.002}_{-0.002}$	$0.018^{+0.002}_{-0.002}$	$0.027^{+0.002}_{-0.002}$	$0.077^{+0.003}_{-0.003}$
MEKAL1	kT	$0.63^{+0.02}_{-0.02}$	$0.65^{+0.01}_{-0.01}$	$0.62^{+0.02}_{-0.02}$	$0.63^{+0.01}_{-0.02}$	$0.64^{+0.02}_{-0.03}$
	Norm $(\times 10^{-4})$	$3.8^{+0.1}_{-0.1}$	$4.1^{+0.2}_{-0.2}$	$3.7^{+0.2}_{-0.2}$	$2.8^{+0.1}_{-0.2}$	$2.6^{+0.2}_{-0.2}$
MEKAL2	kT	$1.59^{+0.13}_{-0.15}$	$1.61^{+0.12}_{-0.19}$	$1.42^{+0.16}_{-0.03}$	$1.42^{+0.09}_{-0.11}$	$1.43^{+0.14}_{-0.09}$
	Norm $(\times 10^{-4})$	$5.5^{+1.0}_{-0.9}$	$6.2^{+1.3}_{-1.6}$	$5.7^{+1.0}_{-0.4}$	$3.8^{+0.8}_{-0.5}$	$4.1^{+0.9}_{-0.4}$
VMCFLOW	$LowT$	$7.8^{+5.6}_{-2.5}$	$7.4^{+0.5}_{-0.5}$	$9.2^{+1.1}_{-0.7}$	$9.2^{+2.2}_{-1.4}$	$9.9^{+0.8}_{-0.9}$
	$HighT$	$22.6^{+1.6}_{-1.0}$	$15.4^{+0.6}_{-0.7}$	$21.7^{+2.0}_{-1.0}$	$43.9^{+3.9}_{-2.6}$	$22.7^{+1.3}_{-1.2}$
	Norm $(\times 10^{-9})$	$9.2^{+9.0}_{-9.0}$	$16.9^{+6.6}_{-1.0}$	$9.0^{+5.0}_{-5.0}$	$4.7^{+0.5}_{-1.4}$	$12.1^{+2.5}_{-2.2}$
Gaussian1 (6.7 keV)	σ	$0.09^{+0.02}_{-0.02}$	$0.06^{+0.03}_{-0.04}$	$0.10^{+0.07}_{-0.02}$	$0.12^{+0.03}_{-0.02}$	$0.09^{+0.02}_{-0.02}$
	Norm $(\times 10^{-5})$	$2.9^{+0.4}_{-0.3}$	$2.2^{+0.4}_{-0.4}$	$2.9^{+0.2}_{-0.3}$	$3.6^{+0.4}_{-0.4}$	$3.1^{+0.4}_{-0.3}$
Gaussian2 (6.9 keV)	σ	0	0	0	0	0
	Norm $(\times 10^{-6})$	$5.5^{+2.1}_{-2.2}$	$5.1^{+1.2}_{-2.1}$	$2.2^{+1.9}_{-2.2}$	$4.2^{+2.1}_{-1.2}$	$3.1^{+2.3}_{-1.8}$
	χ^2_ν (d.o.f)	1.23 (522)	1.23 (538)	1.33 (531)	1.40 (501)	1.30 (531)
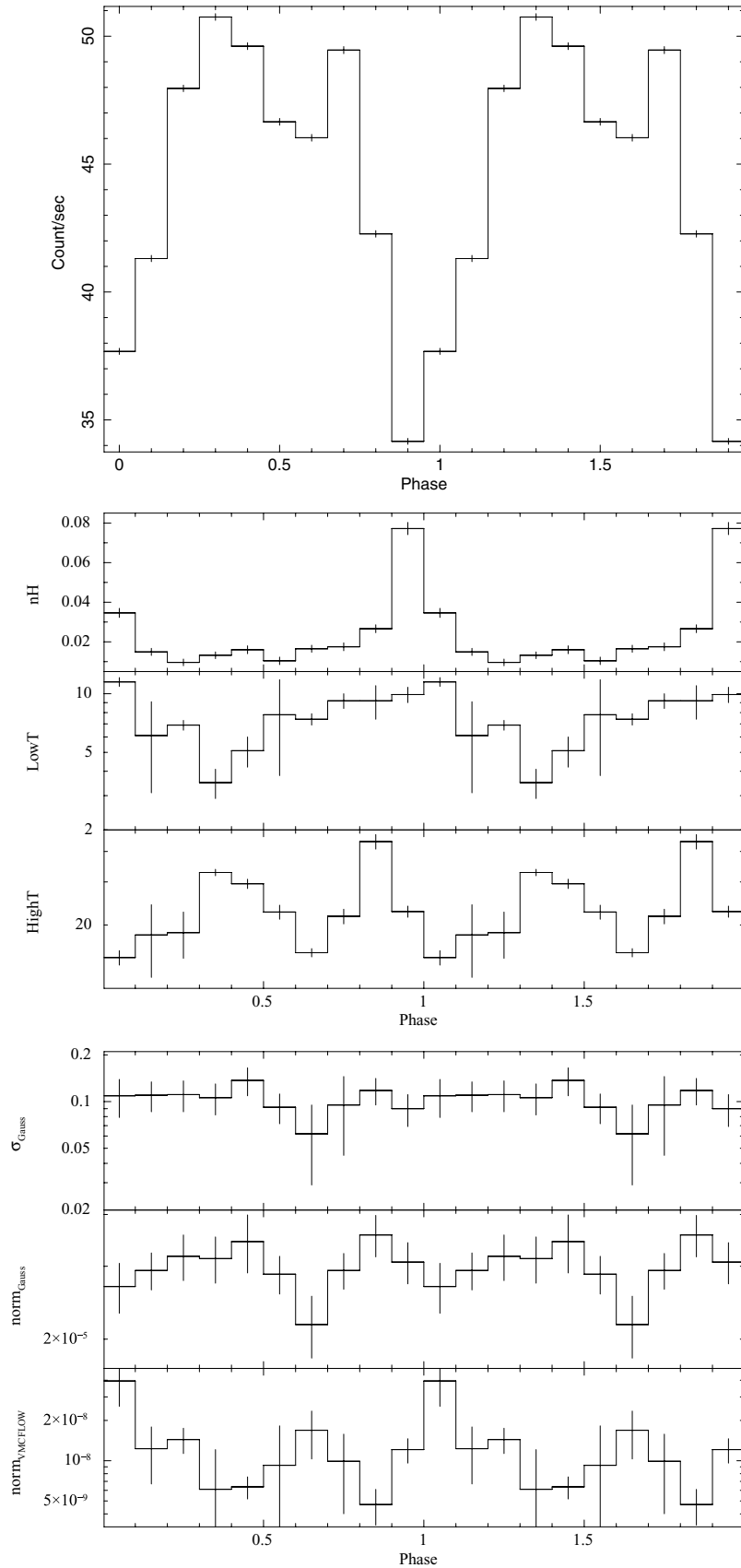
Figure 3. The light curve of the year 2000 data folded over the orbital period of 98 min using the ephemeris $T = 243\,7699.94179 + 0.068233846(4)E$ (top panel) and plots of the spectral parameters derived from the orbital phase-resolved spectroscopy over the same orbital phase range. The σ_{Gauss} and norm $_{\mathrm{Gauss}}$ are parameters for the 6.7-keV line. The lower boundary errors were used in plotting the *highT* parameter.
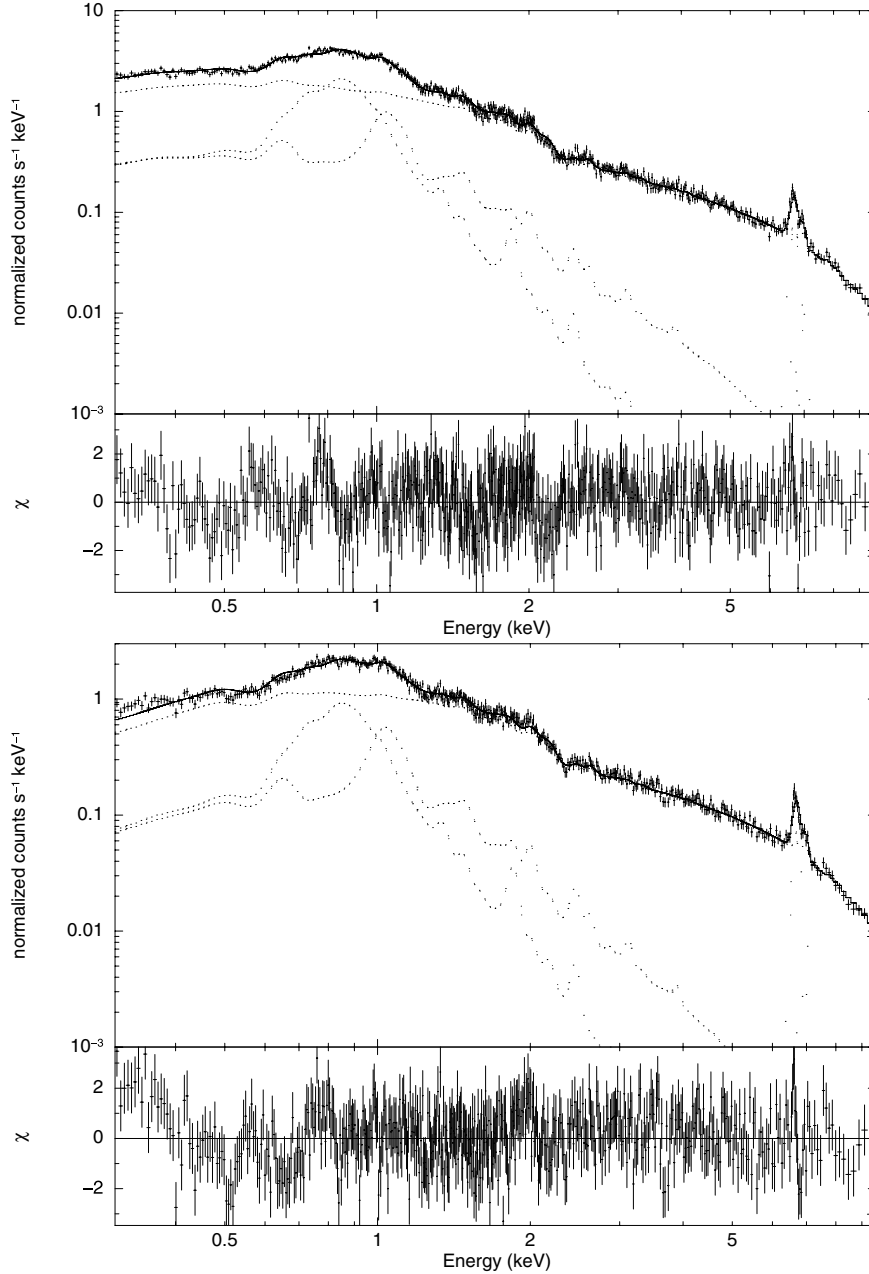
Figure 4. The top panel shows the composite model [WABS*(MEKAL+MEKAL+GAUSS+GAUSS+VMCFLOW)] fitted to the spectrum of orbital maximum (phase 0.3) in the year 2000 data. The bottom panel shows the same composite model fitted to the spectrum of the orbital minimum (phase 0.9) in the year 2000 data. The crosses show the data with error bars, solid lines show the composite model, the dotted lines show the individual models and the panels underneath show the residuals in standard deviations.

at minimum phases by fitting four MEKAL models with variable abundances and focusing on the 6–8 keV regime. The excess around 6.4 keV is clear in Fig. 7. For the orbital maximum (phases between 0.4 and 0.8), the 6.9 and 6.4 keV emission lines could not be fitted with free parameters, however, upper limits for normalizations were obtained by fixing all the other model parameters.

The 6.7-keV linewidths show no distinct variations in the 2000 data, with values around 0.1 keV. On the other hand, in the 2003 data, the widths vary in phase with the flux; the line is broader at the phases of orbital maximum with widths around 0.3 keV, and at phases of orbital minimum it has similar values to the 2000 data,

around 0.1 keV. The width of the 6.4-keV line in the 2003 data varies between 0 and 0.16 keV.

5 SPIN PHASE-RESOLVED SPECTROSCOPY

We have also performed spin phase-resolved spectroscopy in a similar fashion to the orbital phase-resolved spectroscopy for the 2000 and 2003 data. The ephemeris for the spin period $T_0 = 243\,7699.8914(5) + 0.046546504(9)E$ given by Hellier & Sproats (1992) is used for both observations to create spin phase-resolved spectra using the method described in Section 2. XSPEC was used for

Table 4. Spectral parameters derived for the year 2003 observation at each orbital phase of 0.1 in the 0.3–10 keV range. All the spectra were fitted with a composite model of two collisional equilibrium plasma emission models at different temperatures (MEKAL), two Gaussians centred at 6.7 and 6.9 keV, a variable cooling-flow plasma emission model (VMCFLOW) and photoelectric absorption of H I (WABS). In some phases another Gaussian at 6.4 keV was added to the model. The given errors correspond to 2σ confidence level for a single parameter. Gaussian line centres were fixed at their best-fitting values and the iron abundance parameter in VMCFLOW was fixed to 0.2 to improve the quality of the fits.

Model	Component	0.1	0.2	0.3	0.4	0.5
wabs	$N_H (\times 10^{-22})$	$0.142^{+0.006}_{-0.006}$	$0.046^{+0.003}_{-0.003}$	$0.026^{+0.003}_{-0.003}$	$0.020^{+0.002}_{-0.002}$	$0.024^{+0.002}_{-0.002}$
MEKAL1	kT	$0.63^{+0.04}_{-0.06}$	$0.65^{+0.02}_{-0.02}$	$0.61^{+0.03}_{-0.03}$	$0.65^{+0.02}_{-0.02}$	$0.64^{+0.02}_{-0.02}$
	Norm $(\times 10^{-4})$	$1.2^{+0.1}_{-0.2}$	$2.6^{+0.2}_{-0.2}$	$2.6^{+0.3}_{-0.2}$	$3.3^{+0.2}_{-0.2}$	$2.7^{+0.2}_{-0.1}$
MEKAL2	kT	$1.53^{+0.18}_{-0.19}$	$1.80^{+0.26}_{-0.13}$	$1.48^{+0.12}_{-0.08}$	$1.72^{+0.09}_{-0.09}$	$1.65^{+0.14}_{-0.12}$
	Norm $(\times 10^{-4})$	$2.3^{+0.6}_{-0.6}$	$4.3^{+1.3}_{-0.8}$	$3.9^{+0.9}_{-0.8}$	$5.2^{+0.9}_{-0.8}$	$3.6^{+0.8}_{-0.8}$
VMCFLOW	$LowT$	$25.7^{+1.0}_{-5.0}$	$10.8^{+19.5}_{-6.6}$	$4.3^{+1.7}_{-0.9}$	$5.7^{+3.4}_{-1.6}$	$4.1^{+1.4}_{-1.9}$
	$HighT$	$79.9^{<}_{-19.4}$	$60.8^{+12.3}_{-20.2}$	$57.2^{+4.4}_{-2.9}$	$58.2^{+3.2}_{-3.1}$	$60.4^{+3.8}_{-8.5}$
	Norm $(\times 10^{-9})$	$4.1^{+1.4}_{-0.1}$	$4.1^{+1.1}_{-0.8}$	$3.8^{+0.6}_{-0.4}$	$2.7^{+1.0}_{-0.1}$	$3.4^{+0.3}_{-0.2}$
Gaussian1 (6.7 keV)	σ	$0.07^{+0.03}_{-0.03}$	$0.10^{+0.06}_{-0.04}$	$0.10^{+0.09}_{-0.04}$	$0.25^{+0.08}_{-0.05}$	$0.19^{+0.06}_{-0.05}$
	Norm $(\times 10^{-5})$	$3.1^{+0.6}_{-0.5}$	$2.3^{+1.2}_{-0.5}$	$1.4^{+0.9}_{-0.6}$	$3.8^{+0.9}_{-0.8}$	$3.2^{+0.7}_{-0.7}$
Gaussian2 (6.9 keV)	σ	0	0	0	0	0
	Norm $(\times 10^{-6})$	$2.1^{+3.5}_{-2.1}$	$5.1^{+3.7.0}_{-5.1}$	$1.5^{+0.5}_{-0.3}$	<0.000037	<0.000021
Gaussian3 (6.4 keV)	σ	$0.08^{+0.11}_{-0.08}$	$0.09^{+0.44}_{-0.09}$	$0.16^{+0.08}_{-0.06}$	0	0
	Norm $(\times 10^{-6})$	$8.7^{+4.5}_{-5.2}$	$6.3^{+4.7}_{-3.2}$	$14.9^{+4.8}_{-7.3}$	<0.0018	<0.000021
	χ^2_ν (d.o.f.)	1.27 (254)	1.22 (363)	1.40 (380)	1.26 (386)	1.43 (374)

Model	Component	0.6	0.7	0.8	0.9	1.0
wabs	$N_H (\times 10^{-22})$	$0.025^{+0.003}_{-0.002}$	$0.022^{+0.002}_{-0.002}$	$0.020^{+0.002}_{-0.002}$	$0.022^{+0.002}_{-0.002}$	$0.085^{+0.004}_{-0.004}$
MEKAL1	kT	$0.65^{+0.2}_{-0.2}$	$0.63^{+0.02}_{-0.03}$	$0.63^{+0.02}_{-0.02}$	$0.62^{+0.03}_{-0.03}$	$0.67^{+0.07}_{-0.08}$
	Norm $(\times 10^{-4})$	$2.7^{+0.2}_{-0.2}$	$3.0^{+0.2}_{-0.2}$	$3.1^{+0.2}_{-0.2}$	$2.5^{+0.2}_{-0.3}$	$1.0^{+0.2}_{-0.2}$
MEKAL2	kT	$1.64^{+0.11}_{-0.13}$	$1.36^{+0.07}_{-0.07}$	$1.66^{+0.12}_{-0.14}$	$1.35^{+0.08}_{-0.07}$	$1.27^{+0.16}_{-0.14}$
	Norm $(\times 10^{-4})$	$3.9^{+0.8}_{-0.4}$	$2.9^{+0.6}_{-0.4}$	$4.3^{+0.9}_{-0.9}$	$2.4^{+0.7}_{-0.5}$	$1.2^{+0.3}_{-0.3}$
VMCFLOW	$LowT$	$7.3^{+3.4}_{-2.6}$	$3.5^{+1.3}_{-1.0}$	$3.1^{+1.3}_{-1.4}$	$6.9^{+0.8}_{-2.0}$	$24.0^{+0.8}_{-1.0}$
	$HighT$	$73.5^{+4.5}_{-12.5}$	$62.0^{+3.6}_{-3.3}$	$62.0^{+3.7}_{-3.1}$	$79.9^{<}_{-11.8}$	$79.9^{<}_{-14.9}$
	Norm $(\times 10^{-9})$	$3.4^{+0.5}_{-0.4}$	$3.2^{+0.5}_{-0.4}$	$3.4^{+0.9}_{-0.7}$	$3.1^{+0.3}_{-0.2}$	$4.2^{+0.8}_{-0.1}$
Gaussian1 (6.7 keV)	σ	$0.15^{+0.06}_{-0.03}$	$0.20^{+0.05}_{-0.04}$	$0.22^{+0.05}_{-0.04}$	$0.06^{+0.04}_{-0.03}$	$0.08^{+0.04}_{-0.04}$
	Norm $(\times 10^{-5})$	$3.1^{+0.5}_{-0.8}$	$4.4^{+0.8}_{-0.7}$	$4.1^{+0.4}_{-0.7}$	$2.4^{+0.5}_{-0.8}$	$2.2^{+0.6}_{-0.5}$
Gaussian2 (6.9 keV)	σ	0	0	0	0	0
	Norm $(\times 10^{-6})$	<0.00016	<2.3	<1.3	$8.3^{+3.8}_{-3.8}$	$7.9^{+3.7}_{-4.1}$
Gaussian3 (6.4 keV)	σ	0	0	0	$0.0^{+0.3.2}_{>}$	$0.10^{+0.06}_{-0.05}$
	Norm $(\times 10^{-6})$	<0.84	<0.0022	<0.0013	$5.2^{+8.8}_{-3.0}$	$12.1^{+4.9}_{-5.0}$
	χ^2_ν (d.o.f.)	1.17 (385)	1.41 (392)	1.34 (393)	1.44 (376)	1.65 (273)

the remaining spectral analysis, mainly the fitting procedure. The spin phase-resolved spectra were grouped so that each energy bin contained a minimum of 100 counts and data points below 0.3 keV and above 10.0 keV were omitted due to bad statistics.

The ratio of the spin maximum spectra (phases between 0.75 and 0.95) to spin minimum spectra (phases between 0.25 and 0.45) was also studied for the spin phase-resolved spectra. For both the 2000 and 2003 data, the maximum to minimum ratios show similar behaviour, thus there is no difference in the spin phase-resolved spectra, as far as the absorption characteristics are concerned between the two different observations of EX Hya. At low energies, the ratios have values of about 2 that gradually decrease with increasing energy down to 1 (see Fig. 8).

Similar to the previous fits to spectra, two MEKAL models, a VMCFLOW model and various Gaussians to model emission lines were used to fit all the spectra at all spin phases (with 0.1 phase incre-

ments). Differently from the orbital phase-resolved spectroscopy, inclusion of a partial covering absorber model (PCFABS in xspec) was necessary to achieve good fits in the low energies.

The 2003 spin phase-resolved spectra were fitted with xspec models, two MEKAL (collisional equilibrium plasma emission model with solar abundances) at different temperatures, VMCFLOW (cooling-flow model), PCFABS and a Gaussian for the emission line at 6.7 keV. No other emission lines were needed to be included in the fit. Fig. 9 shows the fitted spectra at the spin phase maximum (phase 0.7) and minimum (phases 0.3). Table 5 displays spectral parameters and Fig. 10 is the plot of selected spectral parameters versus the spin phase for the 2003 data. The lower and upper temperature of the cooling flow (i.e. *LowT* and *HighT* parameters of the VMCFLOW model) show anticorrelation with the light curve folded over the spin period. The N_H and the covering fraction of the partial covering absorber parameter does not show a direct
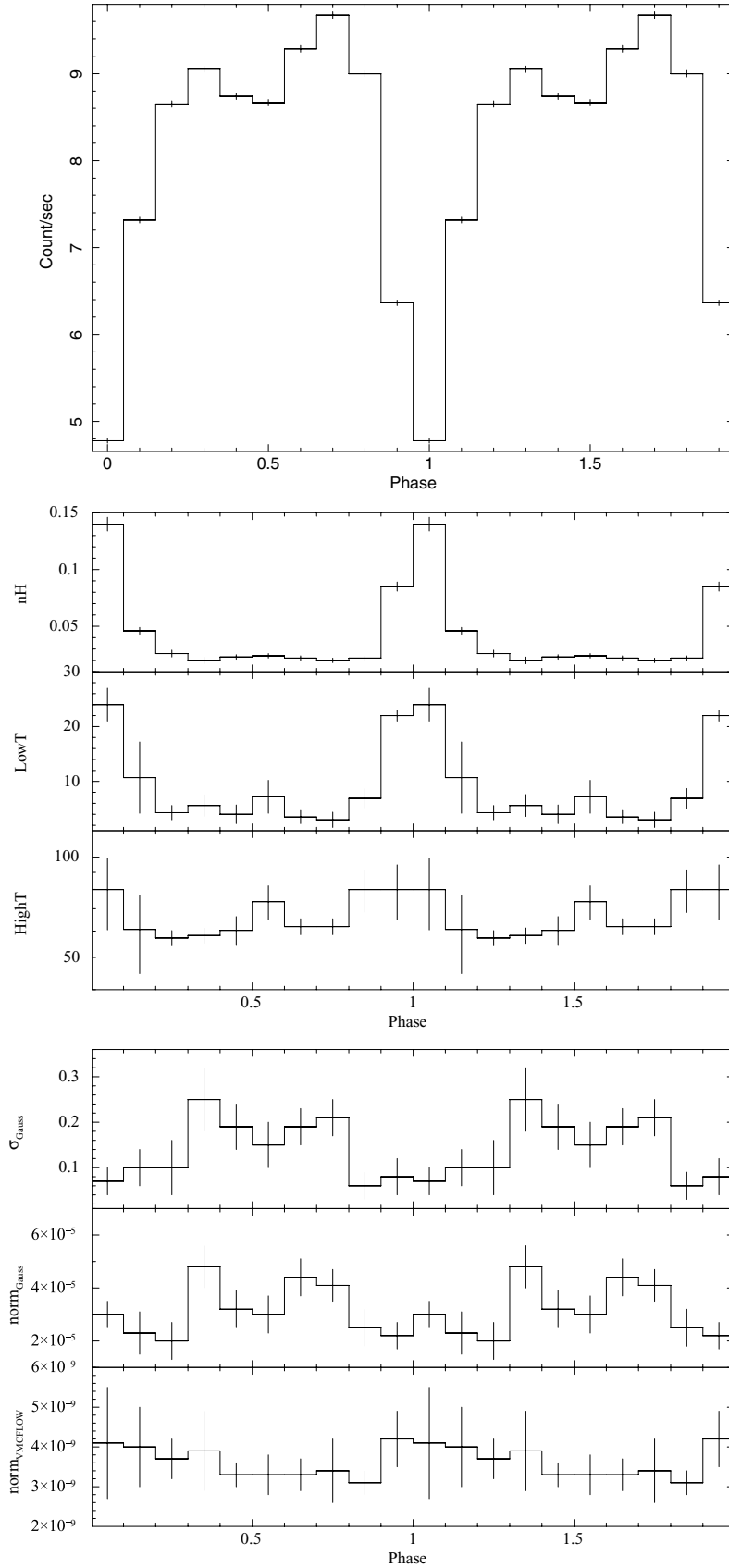
Figure 5. The light curve of the year 2003 data folded over the orbital period of 98 min using the ephemeris $T = 243\,7699.94179 + 0.068233846(4)E$ (top panel) and plots of the spectral parameters derived from the orbital phase-resolved spectroscopy over the same orbital phase range. The σ_{Gauss} and norm $_{\mathrm{Gauss}}$ are parameters for the 6.7-keV line. The lower boundary errors were used in plotting the *highT* parameter.
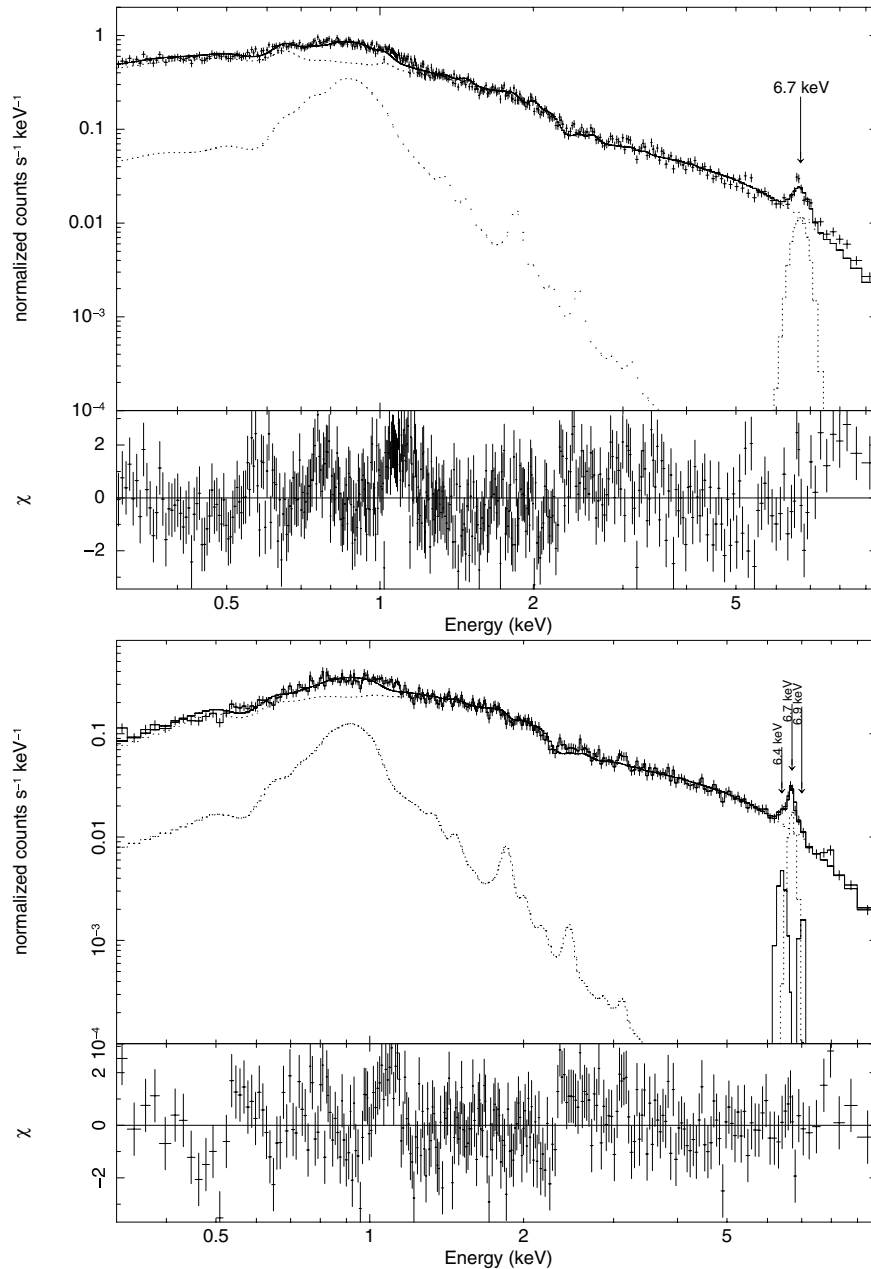
Figure 6. The top panel shows the composite model [PCFABS*(MEKAL+MEKAL+GAUSS+VMCFLOW)] fitted to the spectrum of orbital maximum (phase 0.4) in the year 2003 data. Note that only 6.7-keV line is present. The bottom panel shows the same composite model fitted to the spectrum of the orbital minimum (phase 0) in the year 2003 data. Note that 6.4, 6.7 and 6.9 keV Fe emission lines are present. The crosses show the data with error bars, solid lines show the composite model, the dotted lines show the individual models and the panels underneath show the residuals in standard deviations.

anticorrelation with the flux as would be expected from neutral absorption producing the X-ray modulations. The spectral parameters of the 6.7-keV line do not show any variation over the spin phase. As with the orbital phase-resolved spectroscopy, the need for emission lines were investigated by fitting the data with four MEKAL models with varying abundances and close inspection over the 6–8 keV range. The excess at 6.4 keV does not show any significant pattern as in the orbital phase spectra. The 6.4 and 6.9 keV emission lines could not be fitted with free parameters. However, the upper limits for the 6.4 and 6.9 keV line normalizations could be calculated, with values 1.0×10^{-8} and 5.2×10^{-7} for 6.9 keV and 2.7×10^{-6} and 1.4×10^{-6} for 6.4 keV at minimum flux (phases 0.2 and 0.3); 9.4×10^{-10} and 8.5×10^{-6} for 6.9 keV and 2.3×10^{-6} and 6.0×10^{-7}

for 6.4 keV at maximum flux (phases 0.7 and 0.8). This may be consistent with our results since we find components and emission lines (like the 6.7-keV line) that show widths and normalizations independent of phase generally except for orbital phase in 2003.

The fits to the spin phase-resolved spectra of the 2000 data show that the 6.7 and 6.9 keV emission lines were persistent at all phases. In 2000 data, the parameters N_{H}, covering fraction, *LowT* and *HighT* have higher values during orbital minimum (phases between 0.1 and 0.4) and lower values otherwise showing anticorrelation with the flux. This is the generally expected case if absorption is at work creating the modulations and the spectrum gets harder towards the minimum as the softer photons are absorbed. The spectral
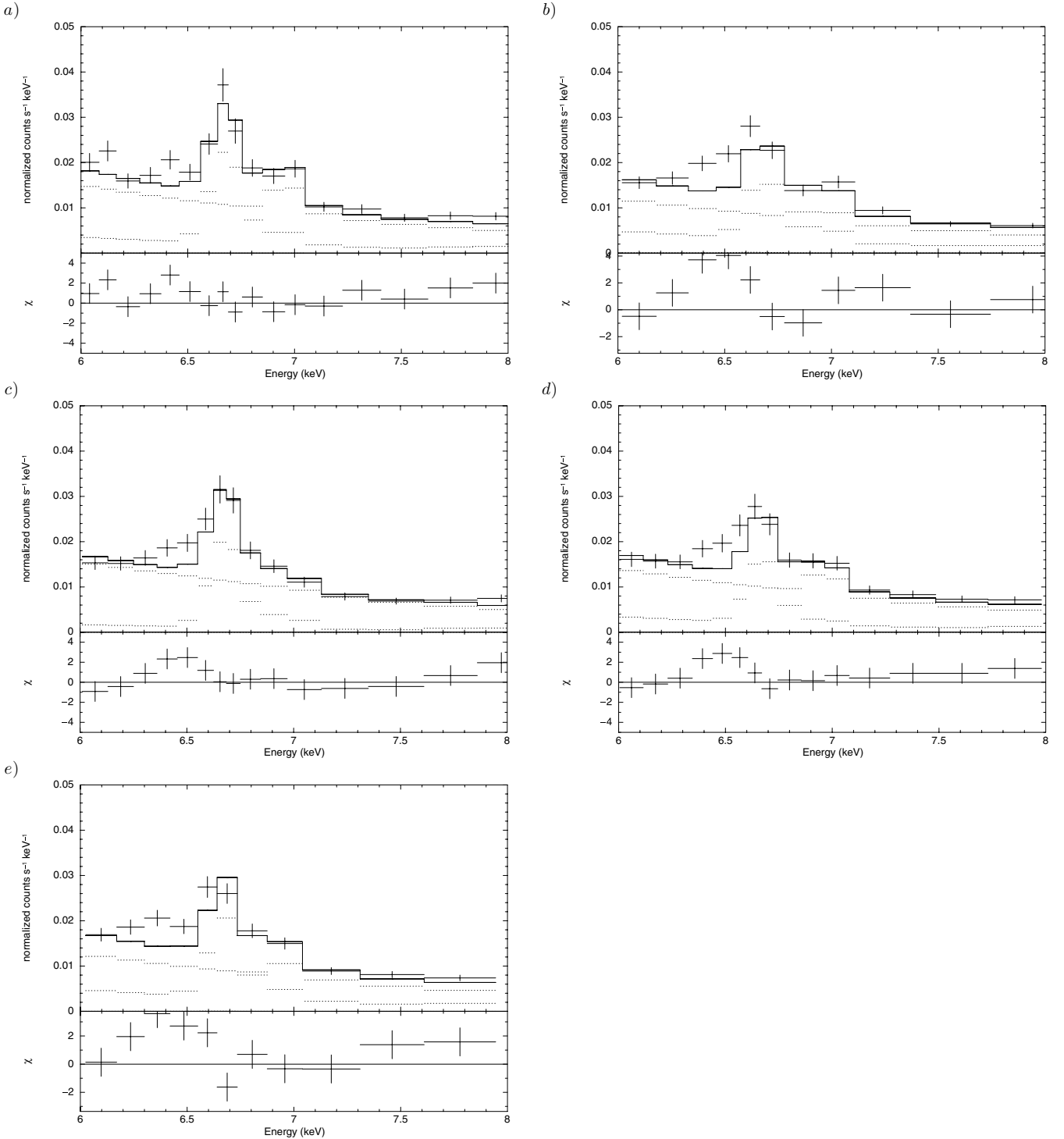
a)

b)

c)

d)

e)

Figure 7. The orbital phase-resolved spectra of 2003 data between phases 0.9 to 1.3 from (a) to (e), respectively. The energy range is between 6 and 8 keV to focus on the emission lines. The spectra were fitted with four MEKAL models to illustrate the excess at 6.4 keV.

parameters of the 6.7-keV line do not show any variation over the spin phase in the 2000 data. The 6.9-keV line is also persistent over the entire range of spin phase except that the normalization minimizes around phases 0.4–0.5 which is about the spin minimum. Fig. 11 shows the fitted spectra at the spin phase maximum (phase 0.9) and minimum (phase 0.5). Table 6 presents the spectral parameters and Fig. 12 displays the plot of selected spectral parameters versus the spin phase.

The MEKAL emission components do not show any significant variation of the temperature parameter over all phases, but a slight variation of the normalization in phase with the spin modulation for both 2000 and 2003 observations is seen.

The widths and normalizations of the emission lines show no significant variation with spin phase for both 2000 and 2003 data, while the width of the 6.7-keV line in 2003 data is slightly larger than that of 2000.
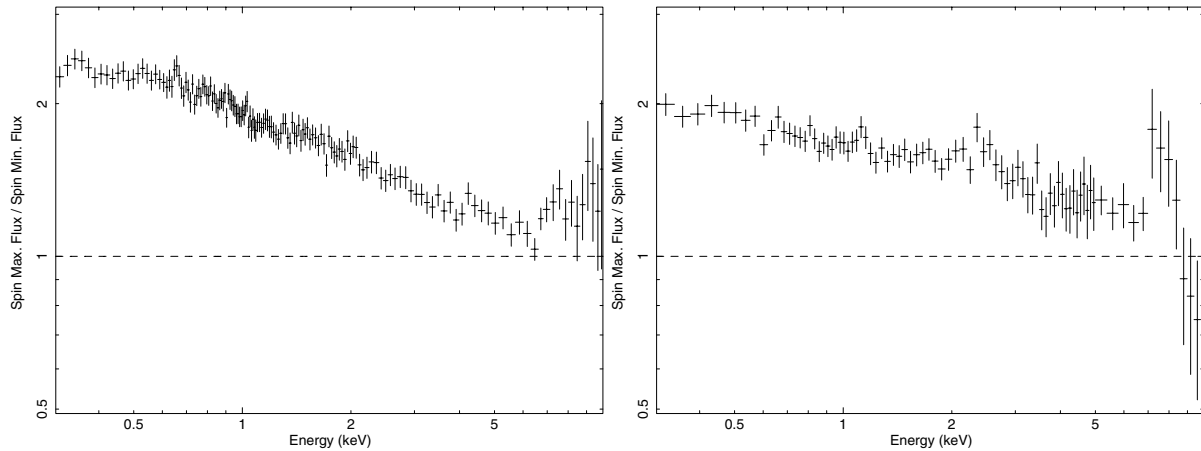
Figure 8. The left-hand panel shows the ratio of the count rate spectrum of the spin maximum phase to the spectrum of the spin minimum phase in the year 2000 data. The right-hand panel shows the ratio of the count rate spectrum of the spin maximum to the spectrum of the spin minimum in the year 2003 data.

6 DISCUSSION

We have presented the *XMM–Newton* EPIC pn data of the IP EX Hya. The spectrum of EX Hya is quite complex as it needs multicomponent emission models to fit the data. For the total spectra of both 2000 and 2003 observations, the composite model is composed of two different MEKAL models with plasma temperatures around 0.6–0.8 and 1.3–1.7 keV, a cooling-flow emission model, VMCFLOW, with a distribution of 3–33 keV for the 2000 observation and 8–61 keV for the 2003 observation, and various Gaussian emission lines at 6.4, 6.7, 6.9, 0.58, 0.78 and 7.8 keV. The 7.8 keV emission line is an unusual feature encountered in the X-ray spectrum of CVs. After a closer investigation around the 5–10 keV spectra of both observations, the line appeared prominently with a centre around $7.8^{+0.3}_{-0.3}$, linewidth of 0.2–0.4 keV and with a normalization of 0.0001 photons cm^{-2} s^{-1}. This line may be the Fe xxv Kβ emission line according to the CHIANTI atomic data base. The emission lines at 0.58 and 0.78 keV correspond to O vii and O viii transitions, respectively. These lines appear only in the phase averaged spectra, hence may be calibration artefacts.

The two different collisional equilibrium plasma emission components around 0.6–0.8 and 1.3–1.7 keV (modelled with MEKAL) are present at all phases (orbital and spin) and in the total spectra. This shows that there is an X-ray emitting region unaffected by orbital and spin phase which may be attributed to an X-ray emission region in the line of sight at all phases. We find that the normalizations of the MEKAL emission components decrease during the eclipse, which indicates that these components originate most likely from the post-shock region in the accretion column which is too complex to be represented with just a cooling-flow plasma emission model alone.

The folded light curve of the source over the orbital period shows two distinct features for both 2000 and 2003 data. The first feature is the eclipse expected to be seen at phases around 0. For the 2000 light curve the eclipse falls at phases 0.93 ± 0.05. Fitting a simple sinusoid to the folded light curve yields a semi-amplitude variation of 6.4 ± 1.0 counts s^{-1} and 14 per cent modulation. For 2003 data the eclipse is at phase 1.02 ± 0.05 with semi-amplitude variation of 1.6 ± 0.3 counts s^{-1} and 20 per cent modulation. The accumulated errors in orbital phase are 0.000083 for 2000 and 0.000088 for 2003 data. With these values, it is clear that the two eclipses do not

overlap, however, early works (e.g. Hoogerwerf et al. 2005) show that the centroid of the eclipse at high energies (i.e. for 10–15 Å it is at phase 0.992) falls behind the eclipse at low energies (i.e. for 15–20 Å it is at phase 1.0). Furthermore, extreme UV (EUV) eclipse was found to be at phase 0.97 by Belle et al. (2002) and it was suggested that the optical eclipse at phase 0 might be due to the eclipse of the hotspot rather than the WD. Hence, the shifting of the eclipse may be to the change in geometry of the eclipsing region between two observations. During the eclipse, the count rate does not drop to zero, which is consistent with a double pole accretion model where the lower accretion column is eclipsed but the upper column is not (Belle et al. 2005). This is consistent with our results since we find components and emission lines (like the 6.7-keV line) that show widths and normalizations independent of any type of phase. However, it is inconclusive since the spin-folded light curves show a single peak profile at all times.

The second prominent feature of the folded mean light curve over the orbital phase is the broad shallow dip appearing in both 2000 and 2003 data. In the 2000 data, the dip is at around phases 0.45–0.65 and roughly 1/3 of the depth of the eclipse. In the 2003 data, the absorption feature is shallower (about 1/5 of the depth of the eclipse) and the location of the dip is around phases 0.35–0.55. This broad modulation was well observed over the optical, UV and X-ray regime and attributed to the bulge and/or hotspot on the disc (e.g. Belle et al. 2005; Hoogerwerf et al. 2005; Mhlahlo et al. 2007a,b). The dip gets stronger and moves to phases closer to the eclipse as the wavelength increases due to the changes in the ionization state of the bulge. In the *RXTE* light curve, the dip is around phase 0.65 (Belle et al. 2005), and in *Chandra* light curve it is around phase 0.78 (Hoogerwerf et al. 2005). Both of these observations are from 2000 May, and the broad dip feature in the 2000 July *XMM–Newton* light curve is in accordance with the above examples. However the feature in 2003 is not consistent. The dip is shallower and at phases further away from the eclipse. This may imply that the source has undergone structural changes between 2000 and 2003 and the bulge has shifted position or grown in size so that modulation is observed at earlier phases. Moreover, the phase-resolved spectra show no significant change in the absorption for either 2000 or 2003 observations, hence the modulation in the orbital light curve cannot be attributed to neutral absorption on the disc.
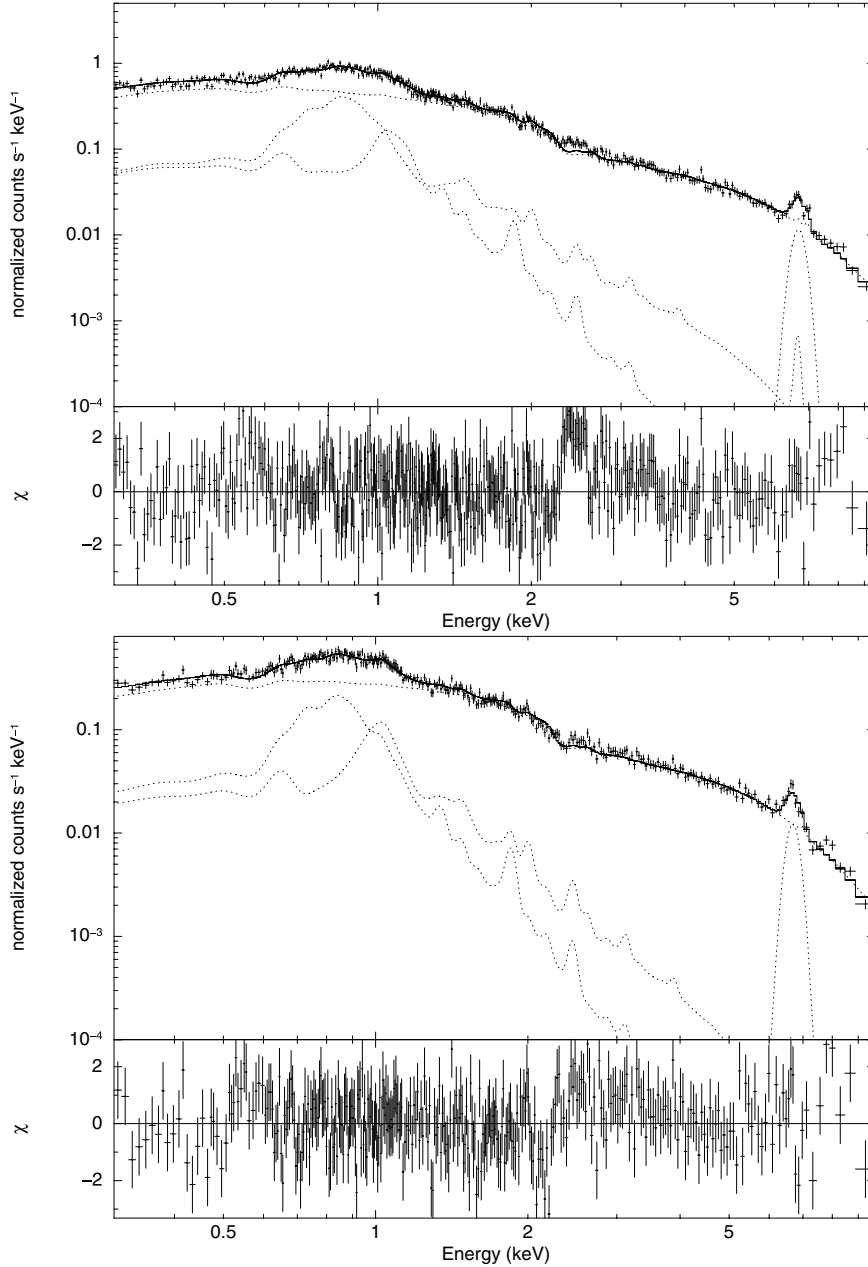
Figure 9. The top panel displays the composite model [PCFABS*(MEKAL+MEKAL+GAUSS+VMCFLOW)] fitted to the spectrum of the spin maximum (phase 0.7) in the year 2003 data. The bottom panel displays the same composite model fitted to the spectrum of the spin minimum (phase 0.3) in the year 2003 data. The crosses show the data with error bars, solid lines show the composite model, the dotted lines show the individual models and the panels underneath show the residuals in standard deviations.

In both 2000 and 2003 data, the neutral absorption and low temperature values of the cooling flow increase significantly during the eclipse. This is an indication that cold absorption plays an important role in the orbital variation of the source. During the eclipse, the absorption increases, reducing the emission from the lower end of the flow and hence the lower temperature values increase. The change in absorption over the orbital motion has been encountered before in another CV; a classical nova RR Pic (Pekön & Balman 2008) where an absorbing region on the disc in the line of sight affects the spectrum. This makes the spectral behaviour of CVs over the orbital period an area worth more investigation.

The light curve folded over the spin period of the WD shows clear sinusoidal modulation for both 2000 and 2003 data. A simple sinusoidal fit shows that the spin minimum is at phase 0.26 ± 0.03, the semi-amplitude variation is 2.1 ± 0.1 counts s^{-1} with 25 per cent modulation for 2003 data. For the 2000 data the minimum is at phase 0.36 ± 0.06, the semi-amplitude variation is 14.5 ± 1.2 counts s^{-1} with 30 per cent modulation. The accumulated errors in phase are 0.0027 for 2000 and 0.0029 for 2003 data, thus they are much smaller than our phase errors. There is a difference in the phase of the spin minimum in different years, most likely due to the changes of the accretion column/curtain structure.

The fits show a net increase of absorption column and covering fraction at the spin minima in the 2000 data indicating the role of absorption from the curtains. Moreover, the low temperature limits of the plasma increase at the phases of minimum flux, making

Table 5. Spectral parameters derived for the year 2003 observation at each spin phase of 0.1 in the 0.3–10 keV range. All the spectra were fitted with a composite model of two collisional equilibrium plasma emission models at different temperatures (MEKAL), a Gaussian centred at 6.7 keV, a variable cooling-flow plasma emission model (VMCFLOW) and a partial covering absorber model (PCFABS). The given errors correspond to 2σ confidence level for a single parameter. Gaussian line centres were fixed at their best-fitting values and the iron abundance parameter in VMCFLOW was fixed to 0.2 to improve the quality of the fits.

Model	Component	0.1	0.2	0.3	0.4	0.5
pcfabs	$N_{\rm H}(\times 10^{-22})$	$0.027^{+0.003}_{-0.029}$	$0.044^{+0.005}_{-0.006}$	$0.093^{+0.044}_{-0.039}$	$0.051^{+0.004}_{-0.006}$	$0.109^{+0.013}_{-0.014}$
	CoverFrac	$1.00^{<}_{-0.16}$	$0.71^{+0.08}_{-0.07}$	$0.68^{+0.08}_{-0.08}$	$0.92^{+0.06}_{-0.06}$	$0.55^{+0.09}_{-0.07}$
MEKAL1	kT	$0.52^{+0.1}_{-0.05}$	$0.63^{+0.02}_{-0.03}$	$0.60^{+0.03}_{-0.04}$	$0.62^{+0.03}_{-0.04}$	$0.62^{+0.02}_{-0.04}$
	Norm $(\times 10^{-4})$	$1.8^{+0.5}_{-0.2}$	$2.2^{+0.2}_{-0.2}$	$1.8^{+0.2}_{-0.2}$	$1.9^{+0.2}_{-0.1}$	$3.2^{+0.8}_{-0.5}$
MEKAL2	kT	$1.10^{+0.28}_{-0.18}$	$1.4^{+0.2}_{-0.1}$	$1.29^{+0.10}_{-0.09}$	$1.58^{+0.08}_{-0.23}$	$1.46^{+0.18}_{-0.10}$
	Norm $(\times 10^{-4})$	$1.9^{+0.2}_{-0.5}$	$1.7^{+0.7}_{-0.4}$	$2.2^{+0.4}_{-0.4}$	$3.3^{+0.7}_{-0.8}$	$2.8^{+0.8}_{-0.6}$
VMCFLOW	*LowT*	$24.1^{+0.4}_{-3.7}$	$26.4^{+0.4}_{-0.9}$	$22.7^{+0.4}_{-2.7}$	$18.1^{+13.1}_{-4.2}$	$6.9^{+2.1}_{-1.4}$
	HighT	$79.9^{<}_{-12.3}$	$79.9^{<}_{-3.8}$	$79.9^{<}_{-11.7}$	$79.9^{<}_{-18.1}$	$79.9^{<}_{-10.3}$
	Norm $(\times 10^{-9})$	$3.8^{+0.7}_{-0.1}$	$3.8^{+0.7}_{-0.1}$	$3.7^{+0.6}_{-0.1}$	$3.7^{+1.8}_{-0.1}$	$3.2^{+1.0}_{-0.1}$
Gaussian1 (6.7 keV)	σ	$0.18^{+0.7}_{-0.5}$	$0.19^{+0.06}_{-0.04}$	$0.18^{+0.04}_{-0.03}$	$0.20^{+0.04}_{-0.04}$	$0.14^{+0.07}_{-0.04}$
	Norm $(\times 10^{-5})$	$3.6^{+0.8}_{-0.6}$	$3.8^{+0.8}_{-0.6}$	$4.2^{+0.7}_{-0.6}$	$4.0^{+0.6}_{-0.7}$	$2.4^{+0.3}_{-0.4}$
	χ^2_ν (d.o.f.)	1.27 (333)	1.21 (312)	1.17 (329)	1.24 (338)	1.35 (360)

Model	Component	0.6	0.7	0.8	0.9	1.0
pcfabs	$N_{\rm H}(\times 10^{-22})$	$0.055^{+0.004}_{-0.005}$	$0.073^{+0.007}_{-0.017}$	$0.069^{+0.043}_{-0.034}$	$0.028^{+0.014}_{-0.002}$	$0.061^{+0.006}_{-0.010}$
	CoverFrac	$0.77^{+0.08}_{-0.13}$	$0.64^{+0.07}_{-0.10}$	$0.48^{+0.29}_{-0.12}$	$1.0^{<}_{-0.14}$	$0.60^{+0.13}_{-0.13}$
MEKAL1	kT	$0.64^{+0.02}_{-0.02}$	$0.64^{+0.02}_{-0.01}$	$0.63^{+0.01}_{-0.01}$	$0.64^{+0.02}_{-0.02}$	$0.64^{+0.02}_{-0.03}$
	Norm $(\times 10^{-4})$	$2.6^{+0.2}_{-0.2}$	$3.4^{+0.3}_{-0.2}$	$3.6^{+0.2}_{-0.2}$	$3.1^{+0.2}_{-0.2}$	$2.6^{+0.2}_{-0.1}$
MEKAL2	kT	$1.67^{+0.12}_{-0.10}$	$1.72^{+0.10}_{-0.13}$	$1.92^{+0.18}_{-0.15}$	$1.66^{+0.18}_{-0.22}$	$1.63^{+0.15}_{-0.16}$
	Norm $(\times 10^{-4})$	$3.8^{+0.9}_{-0.8}$	$4.7^{+1.3}_{-1.0}$	$7.4^{+0.8}_{-0.7}$	$4.8^{+1.2}_{-1.0}$	$3.1^{+0.9}_{-0.8}$
VMCFLOW	*LowT*	$4.1^{+1.0}_{-1.0}$	$3.9^{+0.6}_{-0.5}$	$3.4^{+1.6}_{-1.0}$	$6.2^{+3.0}_{-1.9}$	$8.2^{+3.3}_{-3.7}$
	HighT	$56.7^{+9.0}_{-8.0}$	$43.7^{+18.5}_{-15.7}$	$59.0^{+1.8}_{-2.9}$	$46.4^{+12.7}_{-11.2}$	$61.3^{+3.2}_{-10.3}$
	Norm $(\times 10^{-9})$	$3.6^{+0.7}_{-0.6}$	$4.2^{+0.6}_{-0.5}$	$3.8^{+0.7}_{-0.7}$	$4.7^{+0.9}_{-0.7}$	$4.1^{+1.0}_{-0.9}$
Gaussian1 (6.7 keV)	σ	$0.17^{+0.07}_{-0.04}$	$0.31^{+0.08}_{-0.06}$	$0.15^{+0.09}_{-0.04}$	$0.19^{+0.04}_{-0.04}$	$0.17^{+0.05}_{-0.04}$
	Norm $(\times 10^{-5})$	$3.6^{+0.08}_{-0.06}$	$3.9^{+0.8}_{-0.7}$	$3.5^{+1.0}_{-0.6}$	$4.1^{+0.7}_{-0.7}$	$3.8^{+0.7}_{-0.6}$
	χ^2_ν (d.o.f.)	1.27 (374)	1.46 (396)	1.39 (416)	1.39 (416)	1.55 (382)

the spectrum harder; since absorption reduces the amount of low-temperature X-rays. In the 2003 data the absorption column and covering fraction do not show a clear correlation with the flux, but the low temperature limits of the plasma modulate inversely with the flux. These findings imply that the role of absorption from the accretion curtain is dominant for the source. Although our results do not rule out occultation by the WD as proposed by Allan et al. (1998), the findings favour the absorption effects on the spin modulation to be more dominant.

X-ray spectra of IPs commonly show the fluorescent 6.4 keV emission line feature originating from the reprocessing of the hard X-rays from the WD surface (e.g. Hellier & Mukai 2004; Landi et al. 2009). The 6.4-keV line was encountered in the *Chandra* High Energy Grating (HEG) spectrum of EX Hya (Hellier & Mukai 2004), where the line was weaker than the other lines in the Fe Kα complex (i.e. 6.7 and 6.9 keV emission lines). The total spectrum of the 2003 *XMM–Newton* observations agrees with this, since the normalization of the Gaussian fitted to the 6.4-keV line is less than those of the 6.7 and 6.9 keV emission lines. The behaviour of this fluorescent line over the orbital cycle is however unusual. In the phase-resolved spectra, the line is detected for the orbital and spin phase-resolved spectra of the 2000 observation and the spin phase-resolved spectra of the 2003 data. In the analysis of the 2003 data over the orbital phases, the line is undetected at phases 0.4 to 0.8

(i.e. phases of orbital maxima) but present otherwise (i.e. phases of orbital minima). This means that there is a region on the orbital plane reflecting the X-ray emission seen around the eclipse phases which is a region on the disc rather than the surface of the WD. This reflection phenomenon is detected from a CV and an IP for the first time. We strongly suggest that the bulge at the accretion impact zone will appear at similar binary phases to the eclipse and causes this reflection to occur. Such features are detected in dipping low-mass X-ray binaries (Diaz-Trigo et al. 2006), although with significantly higher linewidths (e.g. $\sigma \sim 0.85$ keV) than seen in this work ($\sigma \sim 0.1$ keV).

It has been shown that a growing number of IPs have a soft blackbody emission component with temperatures less than 100 eV (e.g. Evans & Hellier 2007; Anzolin et al. 2008, 2009; de Martino et al. 2008). EX Hya is listed as a 'soft-IP' by Evans & Hellier (2007) however not with much emphasis, since the spectral fits with a blackbody component yield poor results. Our fits with a blackbody component also give reduced χ^2 values much greater than 2, thus we are also unable to list the source as a 'soft-IP'. There is no need for a soft blackbody component to model the *XMM–Newton* data of EX Hya for both observations.

The cooling-flow plasma emission component yields temperature ranges 3–33 keV (for 2000 data) and 8–61 keV (for 2003 data) in accordance with the high plasma temperatures obtained from other
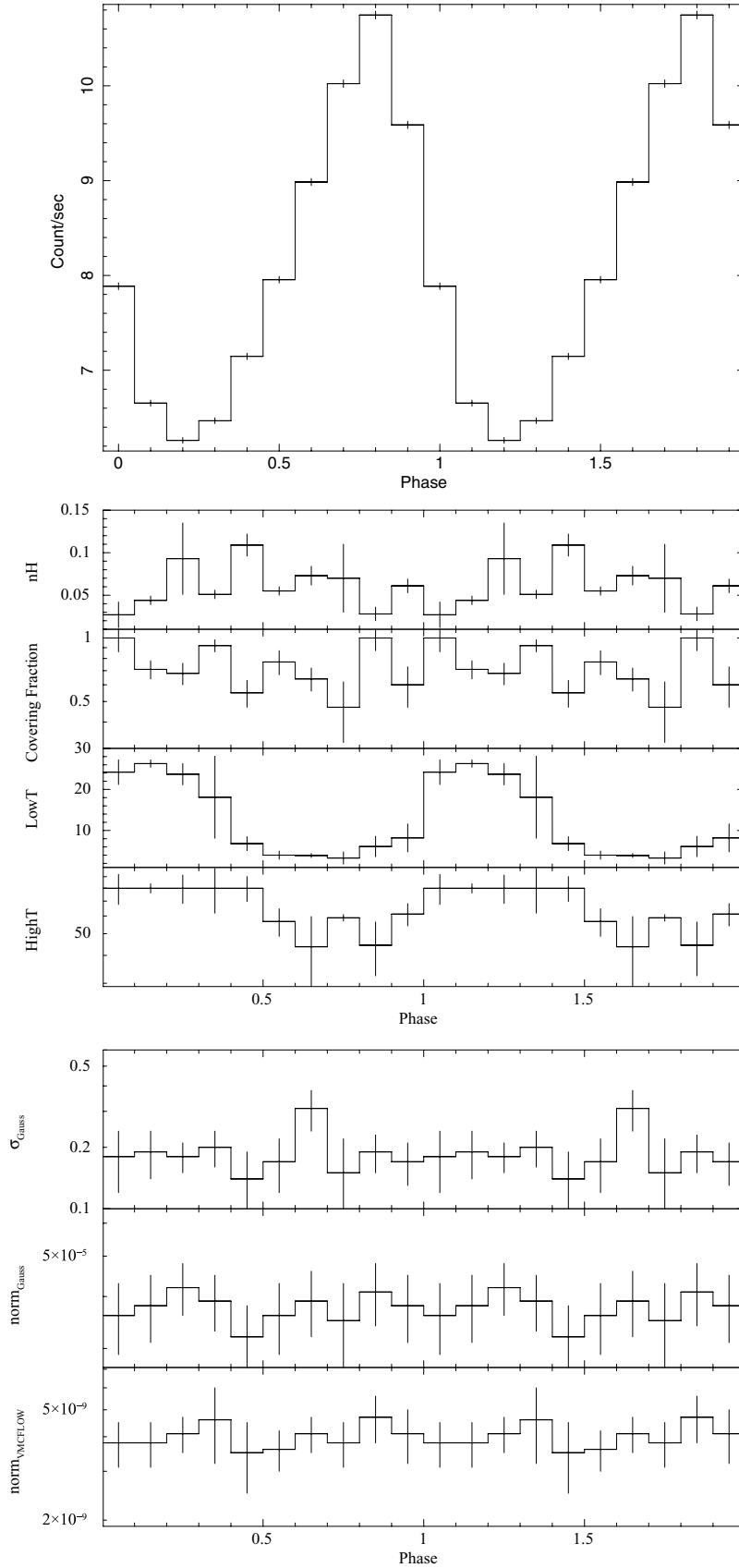
Figure 10. The light curve of the year 2003 data folded over the spin period of 67 min using the ephemeris $T = 243\,7699.8914(5) + 0.046546504(9)E$ (top panel) and plots of the spectral parameters derived from the spin phase-resolved spectroscopy over the same spin phase range. The σ_{Gauss} and norm $_{\mathrm{Gauss}}$ are parameters for the 6.7-keV line. The lower boundary errors were used in plotting the *highT* parameter.
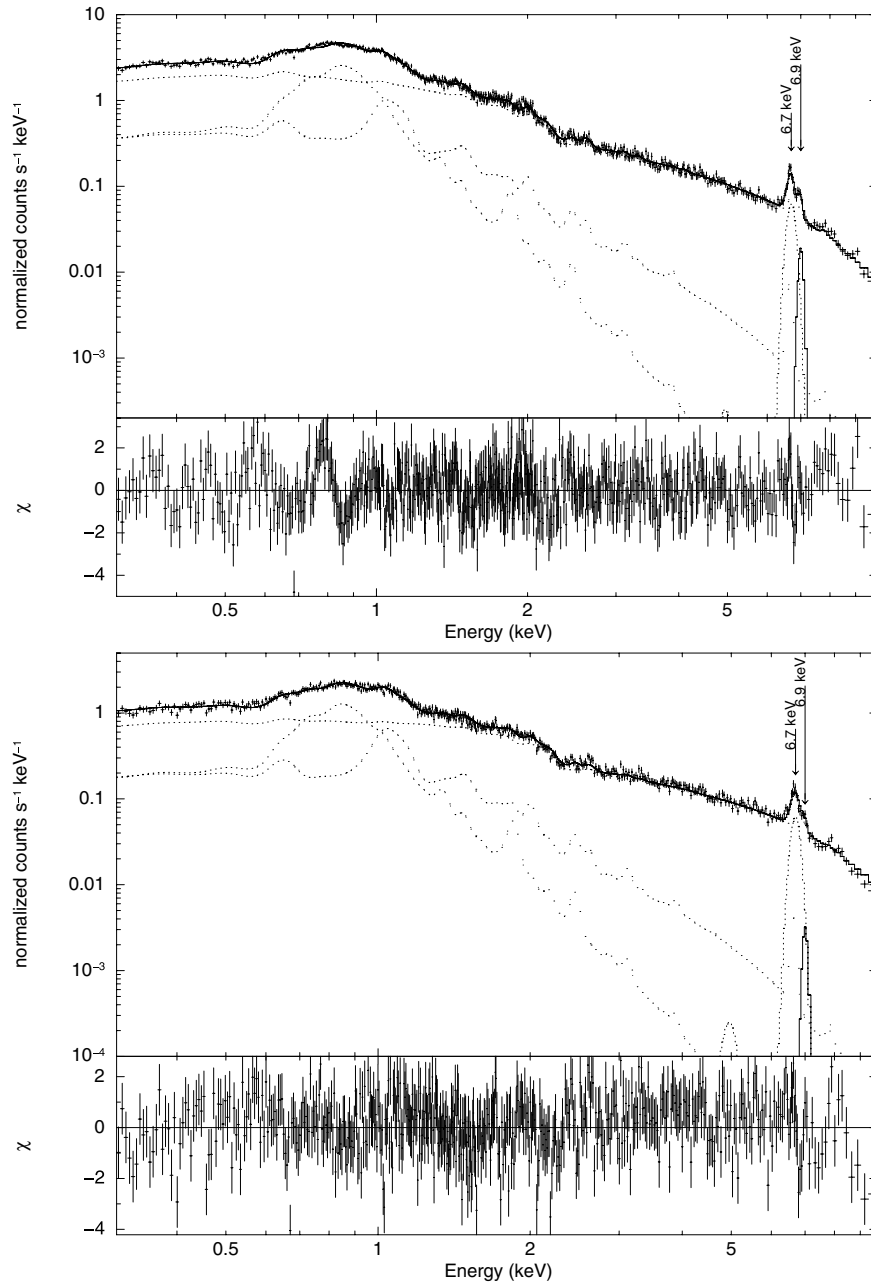
Figure 11. The top panel displays the composite model [PCFABS*(MEKAL+MEKAL+GAUSS+GAUSS+VMCFLOW)] fitted to the spectrum of the spin maximum (phase 0.9) in the year 2000 data. The 6.7 and 6.9 keV emission lines are explicitly shown. The bottom panel displays the same composite model fitted to the spectrum of the spin minimum (phase 0.5) in the year 2000 data. The 6.7 and 6.9 keV emission lines are explicitly shown. The crosses show the data with error bars, solid lines show the composite model, the dotted lines show the individual models and the panels underneath show the residuals in standard deviations.

IPs as expected (e.g. Anzolin et al. 2008, 2009; de Martino et al. 2008). We note that given these observations (e.g. Brunschweiger et al. 2009) EX Hya is one of the IPs that shows the hardest X-ray emission. In previous works with different observations the spectra showed different temperature distributions. Such measurements include 19.4 keV from *Swift* data (Brunschweiger et al. 2009), 0.54–15.4 keV from *ASCA* data (Allan et al. 1998), 12.7 keV from Suzaku data (Yuasa et al. 2010), <20 keV from *Chandra* data (Mukai et al. 2003) and were obtained by fitting plasma models to the spectra, extending up to ∼80 keV (*Chandra* High Energy Transmission Grat-

ing (HETG) data) using measurements of the broad components of emission lines form the pre-shock flow (Luna et al. 2010).

The count rate ratio plots of the spin maximum to minimum and orbital maximum to minimum gives us an idea about the absorber characteristics. The 2000 and 2003 spin ratios are similar, starting at a value about 2 and gradually falling down to 1 with increasing energy. This may imply that the absorption due to the accretion curtain has similar structure in both 2000 and 2003. However, we find that the neutral hydrogen column density is about a factor of 4 larger in the 2000 data compared with that in 2003. So the absorption

Table 6. Spectral parameters derived for the year 2000 observation at each spin phase of 0.1 in the 0.3–10 keV range. All the spectra were fitted with a composite model of two collisional equilibrium plasma emission models at different temperatures (MEKAL), two Gaussians centred at 6.7 and 6.9 keV, a variable cooling-flow plasma emission model (VMCFLOW) and a partial covering absorber model (PCFABS). The given errors correspond to 2σ confidence level for a single parameter. Gaussian line centres were fixed at their best-fitting values and the iron abundance parameter in VMCFLOW was fixed to 0.2 to improve the quality of the fits.

Model	Component	0.1	0.2	0.3	0.4	0.5
pcfabs	$N_{\mathrm{H}}(\times 10^{-22})$	$0.17^{+0.16}_{-0.09}$	$0.06^{+0.12}_{-0.04}$	$0.52^{+0.20}_{-0.25}$	$0.44^{+0.20}_{-0.17}$	$0.20^{+0.08}_{-0.07}$
	CoverFrac	$0.24^{+0.06}_{-0.03}$	$0.31^{+0.68}_{-0.17}$	$0.42^{+0.04}_{-0.04}$	$0.49^{+0.04}_{-0.02}$	$0.43^{+0.07}_{-0.03}$
MEKAL1	kT	$0.62^{+0.2}_{-0.2}$	$0.62^{+0.02}_{-0.02}$	$0.61^{+0.03}_{-0.02}$	$0.62^{+0.01}_{-0.01}$	$0.63^{+0.01}_{-0.03}$
	Norm $(\times 10^{-4})$	$4.6^{+0.4}_{-0.3}$	$3.5^{+0.3}_{-0.2}$	$4.1^{+0.7}_{-0.4}$	$4.4^{+0.7}_{-0.7}$	$3.2^{+0.3}_{-0.4}$
MEKAL2	kT	$1.41^{+0.21}_{-0.07}$	$1.42^{+0.20}_{-0.07}$	$1.41^{+0.22}_{-0.08}$	$1.58^{+0.13}_{-0.16}$	$1.47^{+0.17}_{-0.13}$
	Norm $(\times 10^{-4})$	$5.4^{+1.2}_{-0.6}$	$4.6^{+1.1}_{-0.5}$	$5.7^{+1.1}_{-1.2}$	$6.9^{+1.8}_{-2.4}$	$4.7^{+0.9}_{-0.8}$
VMCFLOW	LowT	$4.2^{+1.3}_{-0.6}$	$11.7^{+3.5}_{-1.9}$	$9.6^{+2.2}_{-1.5}$	$7.1^{+1.2}_{-1.2}$	$5.5^{+1.0}_{-0.6}$
	HighT	$33.8^{+1.3}_{-1.2}$	$45.7^{+5.2}_{-3.3}$	$45.7^{+3.8}_{-3.2}$	$39.4^{+1.2}_{-2.6}$	$35.7^{+2.0}_{-1.3}$
	Norm $(\times 10^{-9})$	$4.6^{+5.5}_{-1.1}$	$4.8^{+1.1}_{-0.8}$	$4.6^{+1.1}_{-0.8}$	$4.9^{+1.6}_{-0.8}$	$5.2^{+2.2}_{-2.2}$
Gaussian1 (6.7 keV)	σ	$0.11^{+0.03}_{-0.01}$	$0.12^{+0.05}_{-0.01}$	$0.10^{+0.04}_{-0.02}$	$0.12^{+0.04}_{-0.02}$	$0.12^{+0.03}_{-0.03}$
	Norm $(\times 10^{-5})$	$2.8^{+0.4}_{-0.4}$	$3.2^{+0.5}_{-0.3}$	$3.2^{+0.4}_{-0.2}$	$3.0^{+0.5}_{-0.4}$	$3.1^{+0.4}_{-0.2}$
Gaussian2 (6.9 keV)	σ	0	0	0	0	0
	Norm $(\times 10^{-6})$	$5.5^{+2.1}_{-2.3}$	$3.4^{+2.1}_{-2.8}$	$4.0^{+2.0}_{-2.4}$	$0.9^{+2.2}_{-0.7}$	$0.9^{+2.0}_{-0.7}$
	χ^2_ν	1.27 (539)	1.26 (493)	1.28 (494)	1.28 (501)	1.23 (494)

Model	Component	0.6	0.7	0.8	0.9	1.0
pcfabs	$N_{\mathrm{H}}(\times 10^{-22})$	$0.12^{+0.06}_{-0.04}$	$0.20^{+0.22}_{-0.11}$	$0.12^{+0.18}_{-0.08}$	$0.12^{+0.07}_{-0.07}$	$0.10^{+0.10}_{-0.06}$
	CoverFrac	$0.46^{+0.10}_{-0.6}$	$0.24^{+0.07}_{-0.03}$	$0.16^{+0.11}_{-0.04}$	$0.22^{+0.13}_{-0.04}$	$0.29^{+0.28}_{-0.07}$
MEKAL1	kT	$0.61^{+0.02}_{-0.02}$	$0.61^{+0.02}_{-0.02}$	$0.62^{+0.02}_{-0.02}$	$0.64^{+0.01}_{-0.01}$	$0.64^{+0.01}_{-0.01}$
	Norm $(\times 10^{-4})$	$3.7^{+0.3}_{-0.2}$	$4.5^{+0.4}_{-0.3}$	$4.9^{+0.3}_{-0.3}$	$6.0^{+0.3}_{-0.3}$	$6.0^{+0.4}_{-0.2}$
MEKAL2	kT	$1.36^{+0.07}_{-0.08}$	$1.40^{+0.10}_{-0.06}$	$1.42^{+0.15}_{-0.06}$	$1.57^{+0.12}_{-0.16}$	$1.71^{+0.10}_{-0.12}$
	Norm $(\times 10^{-4})$	$4.5^{+0.6}_{-0.6}$	$6.1^{+0.4}_{-0.6}$	$7.0^{+0.6}_{-0.6}$	$8.1^{+1.5}_{-1.5}$	$9.3^{+1.7}_{-1.6}$
VMCFLOW	LowT	$2.6^{+0.6}_{-0.5}$	$3.4^{+0.5}_{-0.4}$	$3.7^{+0.6}_{-0.4}$	$2.5^{+0.4}_{-0.4}$	$2.7^{+0.4}_{-0.4}$
	HighT	$34.8^{+1.1}_{-0.9}$	$21.5^{+0.7}_{-0.6}$	$21.6^{+0.7}_{-0.6}$	$22.7^{+0.5}_{-0.5}$	$22.8^{+0.5}_{-0.5}$
	Norm $(\times 10^{-9})$	$4.4^{+6.0}_{-0.5}$	$7.7^{+2.5}_{-2.5}$	$8.9^{+5.2}_{-2.8}$	$8.8^{+4.5}_{-1.4}$	$7.9^{+5.7}_{-1.6}$
Gaussian1 (6.7 keV)	σ	$0.10^{+0.04}_{-0.02}$	$0.10^{+0.03}_{-0.02}$	$0.11^{+0.01}_{-0.02}$	$0.10^{+0.02}_{-0.02}$	$0.11^{+0.03}_{-0.01}$
	Norm $(\times 10^{-5})$	$3.1^{+0.5}_{-0.3}$	$2.7^{+0.4}_{-0.3}$	$3.2^{+0.4}_{-0.4}$	$3.2^{+0.4}_{-0.4}$	$3.0^{+0.4}_{-0.4}$
Gaussian2 (6.9 keV)	σ	0	0	0	0	0
	Norm $(\times 10^{-6})$	$4.2^{+1.9}_{-2.5}$	$4.6^{+2.0}_{-2.2}$	$5.6^{+2.2}_{-2.4}$	$5.3^{+2.1}_{-2.3}$	$5.0^{+2.4}_{-2.6}$
	χ^2_ν	1.31 (521)	1.39 (527)	1.22 (581)	1.10 (600)	1.24 (583)

in the accretion column/curtain is removed to some extent in the 2003 data. The orbital spectral ratios show a significant difference in the years 2000 and 2003. They both show a power-law decay over the *XMM–Newton* energy range, where the 2000 data are flatter and the 2003 data show a prominent decay in the ratio over the *XMM–Newton* energy range.

So there is a clear difference between 2000 and 2003 states of the source as far as absorption over the orbital cycle is concerned. This most probably due to the changing geometry and ionization structure of the absorbing material on the binary plane/accretion disc.

The estimates from the model integrated fluxes yielded luminosities of 6.7×10^{31} and 5.8×10^{31} erg s^{-1} and accretion rates of 5.75×10^{-11} and 5.0×10^{-11} M$_\odot$ yr^{-1} for 2000 and 2003 data, respectively. The X-ray luminosities are lower but the accretion rates are in accordance with the previous findings of Beuermann et al. (2003) from optical data. We find that this region is located around the accretion impact zone creating a sizeable absorbing bulge in a similar fashion to low-mass X-ray binary systems. This region has

a smaller neutral hydrogen column density by at least a factor of 4 in the year 2000 and affects a smaller range of phases, but it still exists.

7 SUMMARY AND CONCLUSIONS

The *XMM–Newton* EPIC pn (0.3–10.0 keV) spectrum of the IP EX Hya together with spin and orbital phase-resolved spectroscopy were thoroughly investigated for the first time in this work. We have used two different observations of EX Hya to look for spectral variations over time. In both observations the mass accretion rate and luminosities are compatible with those of the previous quiescent observations, hence the source is in a quiescent state both in 2000 and 2003. The X-ray emission is modelled as arising from three different components: two collisional equilibrium plasma emission models around 0.6–0.8 and 1.3–1.7 keV and a cooling-flow plasma emission model with a distribution of 3–33 keV for the 2000 state and 8–61 keV for the 2003 state. We find very little change in the spectral parameters of the two collisional equilibrium plasma
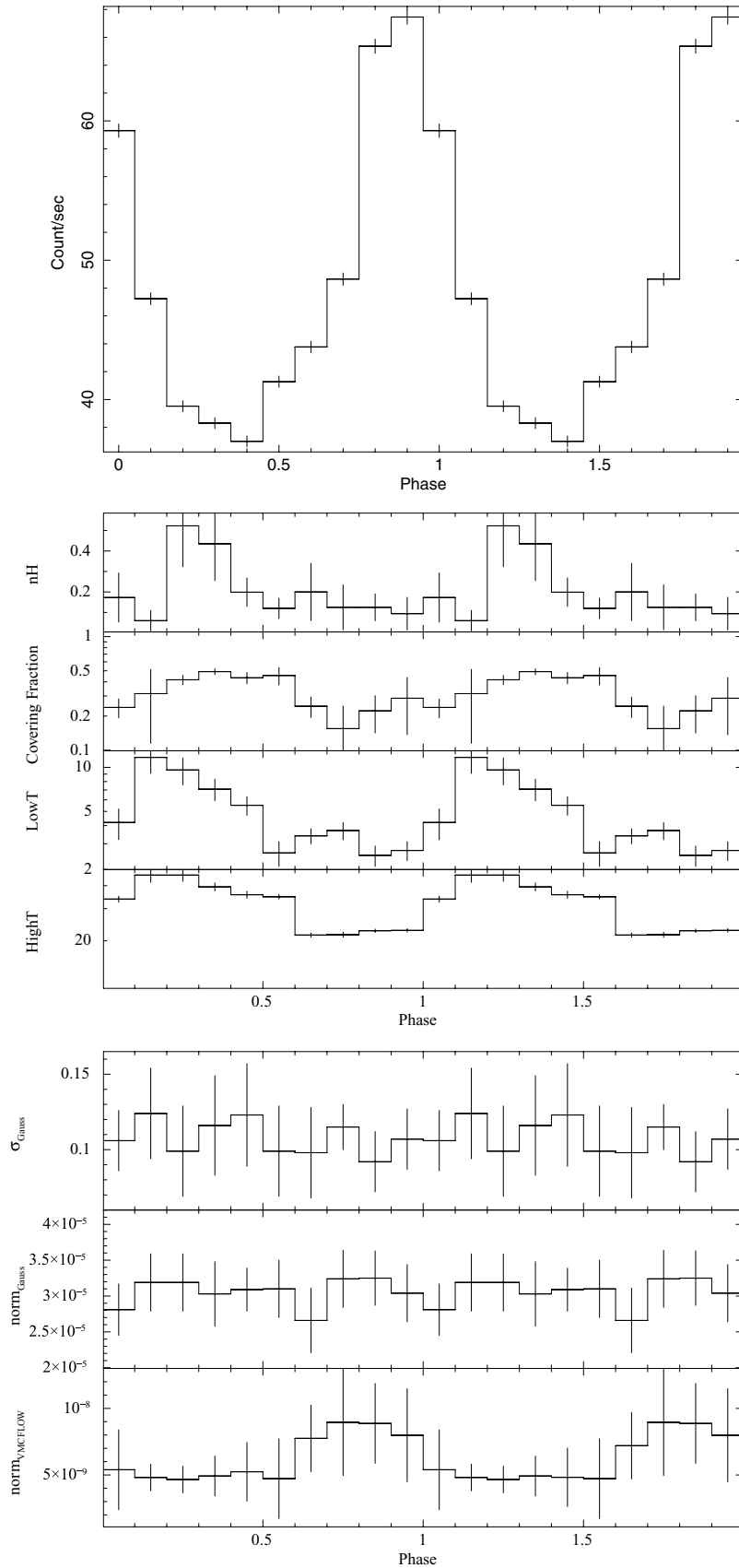
Figure 12. The light curve of the year 2000 data folded over the spin period of 67 min using the ephemeris $T = 243\,7699.8914(5) + 0.046546504(9)E$ (top panel) and plots of the spectral parameters derived from the spin phase-resolved spectroscopy over the same spin phase range. The $\sigma_{\rm Gauss}$ and norm $_{\rm Gauss}$ are parameters for the 6.7-keV line. The lower boundary errors were used in plotting the *highT* parameter.

emission models over the orbital and spin cycles. In general, the two observations of the source reveal spectral variations. For the 2000 data, we find neutral hydrogen column densities in a range 0.01–0.2×10^{22} cm^{-2} from spin phase-resolved spectroscopy (with covering fractions ranging from 0.2 to 0.5), and 0.01–0.08×10^{22} cm^{-2} from orbital phase-resolved spectroscopy (where covering fraction is 1.0). For the 2003 data, the neutral hydrogen column densities are in a range 0.03–0.1×10^{22} cm^{-2} (with covering fractions of 0.6–1.0) in the spin resolved spectroscopy, and 0.02–0.15×10^{22} cm^{-2} in the orbital phase-resolved spectroscopy (with covering fraction of 1.0). The highest N_H values always occur either at the orbital or spin phase minima. There is a definite difference in the absorber geometry for the spin phase-resolved spectroscopy between the two epochs. In the year 2000 it shows a covering fraction of 0.2–0.5 whereas in the year 2003 it shows a covering fraction of 0.6–1.0 (both years show that covering fraction reduces towards spin maxima). This indicates a geometrical change in the absorber from 2000 to 2003. The angle subtended by the absorber is considerably less in 2000 and hence the accretion curtain is reduced in size. Since we attained a model of only neutral absorption, we cannot comment much on the ionization state changes of the absorber. We note that we do not rule out any occultation effect or change in the occultation effects. The absorption in the orbital plane changes by a factor of 2 from 2000 to 2003 and the absorption effects are more spread over the orbital cycle in comparison with the 2000 data. Thus, the bulge at the accretion impact zone is larger (and optically thicker) in 2003. We also note that both the spin and orbital phase-resolved spectroscopy of the 2003 data show a larger variation (3–25 keV) for the *LowT* parameter of the cooling-flow plasma emission model as compared to the 2000 state where this parameter stays around 6–12 keV over most of the phase-resolved spectroscopy. Thus, the structure of the cooling flow and the absorption effects is different in the two different epochs of observations. This is not related to any mass accretion rate difference, but only to a difference in the accretion column temperature distribution structure and absorption.

We detect a 6.4 keV fluorescent Fe line at orbital phases 0.9–1.3 corresponding to the location of orbital minima in 2003 and it is absent in the orbital phases 0.4 to 0.8. This feature can be attributed to reflection from a region on the orbital plane most likely the bulge at the accretion impact zone and spread around the disc covering a location including the eclipse phases. So the absorber may be viewed in other wavelengths at around these phases. We note that a 6.4 keV fluorescent Fe line is non-existent in the orbital phase-resolved spectroscopy of the 2000 data. This strongly indicates an accretion geometry change and a change in the bulge size (impact zone) from year 2000 to 2003; the bulge is larger and more spread in 2003.

REFERENCES

Allan A., Hellier C., Beardmore A., 1998, MNRAS, 295, 167
Anzolin G., de Martino D., Bonnet-Bidaud J.-M., Mouchet M., Gänsicke B. T., Matt G., Mukai K., 2008, A&A, 489, 1243
Anzolin G., de Martino D., Falanga M., Mukai K., Bonnet-Bidaud J.-M., Mouchet M., Terada Y., Ishida M., 2009, A&A, 501, 1047
Arnaud K. A., 1996, in Jacoby G., Barnes J., eds, ASP Conf. Ser. Vol. 101, Astronomical Data Analysis Software and Systems V. Astron. Soc. Pac., San Francisco, p. 17
Barlow E. J., Knigge C., Bird A. J., Dean A. J., Clark D. J., Hill A. B., Molina M., Sguera V., 2006, MNRAS, 372, 224
Belle K. E., Howell S. B., Sirk M. M., Huber M. E., 2002, ApJ, 577, 359
Belle K. E., Howell S. B., Mukai K., Szkody P., Nishikida K., Ciardi D. R., Fried R. E., Oliver J. P., 2005, AJ, 129, 1985
Beuermann K., Harrison Th. E., McArthur B. E., Benedict G. F., Gansicke B. T., 2003, A&A, 412, 821
Brunschweiger J., Greiner J., Ajello M., Osborne J., 2009, A&A, 496, 121
Cropper M., Ramsay G., Hellier C., Mukai K., Mauche C., Pandel D., 2002, R. Soc. Philos. Trans. A, 360, 1951
de Martino D. et al., 2008, A&A, 481, 149
den Herder J. W. et al., 2001, A&A, 365, 7
Diaz-Trigo M., Parmar A. N., Boirin L., Méndez M., Kaastra J. S., 2006, A&A, 445, 179
Evans P. A., Hellier C., 2007, ApJ, 663, 1277
Fujimoto R., Ishida M., 1997, ApJ, 474, 774
Hellier C., 1996, in Evans A., Wood J. H., eds, Cataclysmic Variables and Related Objects. Kluwer, Dordrecht, p. 143
Hellier C., Mukai K., 2004, MNRAS, 352, 1037
Hellier C., Sproats L. N., 1992, Inf. Bull. Var. Stars, 3724, 1
Hellier C., Mason K. O., Rosen S. R., Cordova F. A., 1987, MNRAS, 228, 463
Hoogerwerf R., Brickhouse N. S., Mauche C. W., 2005, ApJ, 628, 946
Jansen F. et al., 2001, A&A, 365, 1
Kraft R. P., 1962, ApJ, 135, 408
Landi R., Bassani L., Dean A. J., Bird A. J., Fiocchi M., Bazzano A., Nousek J. A., Osborne J. P., 2009, MNRAS, 392, 630
Luna G. J. M., Raymond J. C., Brickhouse N. S., Mauche C. W., Proga D., Steeghs D., Hoogerwerf R., 2010, ApJ, 711, 1333
Mason K. O. et al., 2001, A&A, 365, 36
Mhlahlo N., Buckley D. A. H., Dhillon V. S., Potter S. B., Warner B., Woudt P. A., 2007a, MNRAS, 378, 211
Mhlahlo N., Buckley D. A. H., Dhillon V. S., Potter S. B., Warner B., Woudt P. A., 2007b, MNRAS, 380, 353
Mukai K., Kinkhabwala A., Peterson J. R., Kahn S. M., Paerels F., 2003, ApJ, 586, 77
Norton A. J., Wynn G. A., Somerscales R. V., 2004, ApJ, 614, 349
Norton A. J., Butters O. W., Parker T. L., Wynn G. A., 2008, ApJ, 672, 524
Paterson J., 1994, PASP, 106, 209
Pekön Y., Balman Ş., 2008, MNRAS, 388, 921
Rosen S. R., Mason K. O., Cordova F. A., 1988, MNRAS, 231, 549
Scaringi S. et al., 2010, MNRAS, 401, 2207
Strüder L. et al., 2001, A&A, 365, 18
Turner M. J. L. et al., 2001, A&A, 365, 27
Vogt N., Krzeminski W., Sterken C., 1980, A&A, 85, 106
Warner B., 2003, Cataclysmic Variable Stars. Cambridge Univ. Press, Cambridge
Yuasa T., Nakazawa K., Makishima K., Saitou K., Ishida M., Ebisawa K., Mori H., Yamada S., 2010, A&A, 520, 25

This paper has been typeset from a TeX/LaTeX file prepared by the author.